www.thieme.com

SYNTHESIS
Reviews and Full Papers in Chemical Synthesis

Publishing House and Copyright:
© 2024 by
Georg Thieme Verlag KG
Rüdigerstraße 14
70469 Stuttgart
ISSN 0039-7881

Thieme

Synthesis C. M. Matherne et al. Paper

Palladium Nano-Dispersed and Stabilized in Organically Modified Silicate as a Heterogeneous Catalyst for the Conversion of Aldehydes into *O*-Silyl Ether Derivatives under Neat Conditions

Caitlyn M. Matherne[◊a]
Jordan E. Wroblewski[◊a]
Heather S. Drago[a]
Gabriela T. Marchan[a]
Alexis R. Young[a]
Nkechi Kingsley[b]
Craig P. Plaisance[b]
Jean Fotie*[a]

[a] Department of Chemistry and Physics, Southeastern Louisiana University, SLU 10878, Hammond, LA 70402-0878, USA
jean.fotie@selu.edu
[b] Cain Department of Chemical Engineering, Louisiana State University, Baton Rouge, LA 70803, USA
nkings1@lsu.edu
[◊] These authors contributed equally

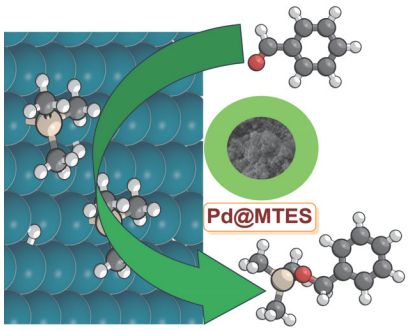

Received: 02.04.2024
Accepted after revision: 14.05.2024
Published online: 14.05.2024 (Accepted Manuscript), 04.06.2024 (Version of Record)
DOI: 10.1055/a-2326-6277; Art ID: SS-2024-04-0114-OP

Abstract Palladium nanoparticles are dispersed and stabilized in organically modified silicate (Pd@MTES), and characterized by a number of spectroscopic techniques, including FTIR, TEM, SEM, and XPS. The catalytic effect of this material toward the hydrosilylation of aldehydes and ketones is explored, and the scope of the reaction investigated, with 26 examples provided. This reaction proceeds under neat conditions via heterogeneous catalysis, and a mechanistic pathway supported by DFT calculations is proposed.

Key words palladium nanoparticles, hydrosilylation, aldehydes, ketones, heterogeneous catalysis, DFT calculations

The increasing involvement of heterogeneous catalytic systems in the development of more efficient and environmentally friendly chemical transformations, driven by the emergence of industrial continuous processes, is an evolving area of catalysis.[1,2] In fact, the development of active, selective, and energy-efficient catalytic processes is believed to be key to a sustainable future by accelerating the transition to a carbon-neutral society.[3] As continuous flow processes, which offer many advantages over traditional batch reactors, including a high surface-to-volume ratio, better heat and mass transfer, and more control over reaction conditions,[4] become more prevalent in the chemical industry, there is a need for the development of a new generation of catalysts compatible with these processes. Therefore, the design, evaluation, and implementation of robust and selective heterogeneous catalytic processes controlled by solid surfaces could have a tremendous positive impact on the world.[1]

One approach compatible with these greener and sustainable industrial practices consists of the heterogenization of homogeneous catalytic methods through the dispersion or encapsulation of metallic nanoparticles in porous matrices.[5–10] This approach, in addition to offering a unique high specific surface area and large pore volume, along with the tunability of pore size, also enables easy product separation and catalyst reusability.[11–13] Because of the rigid-glassy nature of silica-based sol-gels, added to the fact that they are extremely porous materials with high specific area, nano-dispersed and stabilized metallic catalysts in organically modified silicates have been investigated as potential catalysts for continuous flow processes.[7,14]

As the second most naturally abundant element on earth, it is only intuitive for silicon-based materials to be widely used in a large number of consumer goods and commodity chemicals, including polymers (adhesives,[15] gels,[16] encapsulants,[17] coatings,[18] and sealants[19]), semiconductors,[20] and biomedical agents,[21] to name just a few. As such, hydrosilylation reactions have become increasingly popular as a preferred method to produce organosilanes and organosilicons, and while the hydrosilylation of olefins and alkynes is more prevalent,[5,22] a great deal of attention has also been paid to the hydrosilylation of aldehydes and ketones.[23,24]

Organically modified silicates (ORMOSILs) are mesoporous structures with a uniquely large specific surface area, high thermal stability, and large pore volume, along with the convenience of tunable pore size.[12,13,25,26] Their preparation is straightforward from readily available and non-toxic hydrosilanes, with the presence of heteroatoms at the organic linkers within these materials making them effective stabilizers for metal nanoparticles.[5,25,27] In our continuous effort to develop catalytic systems compatible with industrial flow systems,[5] we herein report a catalytic system based on palladium nanoparticles dispersed and stabilized in organically modified silicates (Pd@MTES) for the hydrosilylation of aldehydes and ketones, operating under heterogeneous catalysis.

Since ORMOSILs often generate polyhedral oligomeric frameworks, they are among some of the relatively interesting organic–inorganic hybrid materials because their molecular structures contain the smallest inorganic Si–O core covalently bonded to organic substituents.[8,10,28,29] In this study, Pd@MTES was prepared by dispersing a solution of palladium nitrate dihydrate [$(Pd(NO_3)_2{\cdot}2H_2O$] in a hydrolyzed and polymerized triethoxymethylsilane sol-gel, followed by on-site reduction to Pd(0) with the addition of $NaBH_4$ as previously described,[5,9] and the obtained material was characterized using a wide range of techniques. Figure 1 shows the FT-IR spectra of trihydroxymethylsilane, the hydrolyzed and non-polymerized triethoxymethylsilane (purple), and that of the resulting homogeneous condensed sol-gel after the distribution and encapsulation of palladium nanoparticles in the inner porosity of the three-dimensional siloxane network (Pd@MTES, in red), respectively.

The signals observed in the FT-IR spectra of both trihydroxysilane and the organically modified silicate material are in full alignment with the previously reported data from the literature related to the characterization of organically modified silicate sol-gels.[10,28–30] The broad signal at ~3331 cm^{-1} attributable to ν(OH) and the corresponding bending band for ν(Si–OH) at ~915 cm^{-1}, added to the bending vibration signals for ν(O–Si–O) observed at ~1082 cm^{-1} and ~1042 cm^{-1}, confirmed the presence of free hydroxy groups connected to the silicon atom in the FT-IR spectrum of trihydroxymethylsilane. Additional signals, including those assigned to the stretching vibration of the methyl groups bonded to silicon at ~2975 cm^{-1} for ν($CHsp^3$) and at ~1269 cm^{-1} for ν(Si–C), together with the bending signals at ~776 cm^{-1} assigned to ν[$(Si)CH_3$], are further confirmation of the complete hydrolysis of triethoxymethylsilane into trihydroxymethylsilane.

After the dispersion of palladium nanoparticles and the polymerization of trihydroxymethylsilane into a gel, the resulting catalyst was characterized by FT-IR as well, with the obtained spectrum provided in Figure 1. The assignment of the respective signals in comparison to those observed in the IR spectrum of the hydrolyzed and non-polymerized triethoxymethylsilane (trihydroxymethylsilane) is also provided in Table 1. In fact, the respective signals associated with the free hydroxy groups, namely the broad signal at ~3331 cm^{-1} for ν(OH) and the corresponding bending band for ν(Si–OH) at ~915 cm^{-1}, are absent in the IR spectrum of the material obtained after the polymerization and formation of the condensed sol-gel. However, the stretching signals for ν($CHsp^3$), ν(Si–C), ν(O–Si–O), and the bending signals for ν[$(Si)CH_3$] were all present in both IR spectra, confirming the formation of the core siloxane matrix. This is a clear indication that the polymerization of trihydroxymethylsilane was completed, and that the metal nanoparticles are indeed dispersed and stabilized in the homogeneous three-dimensional silicate network.[10,29,31]

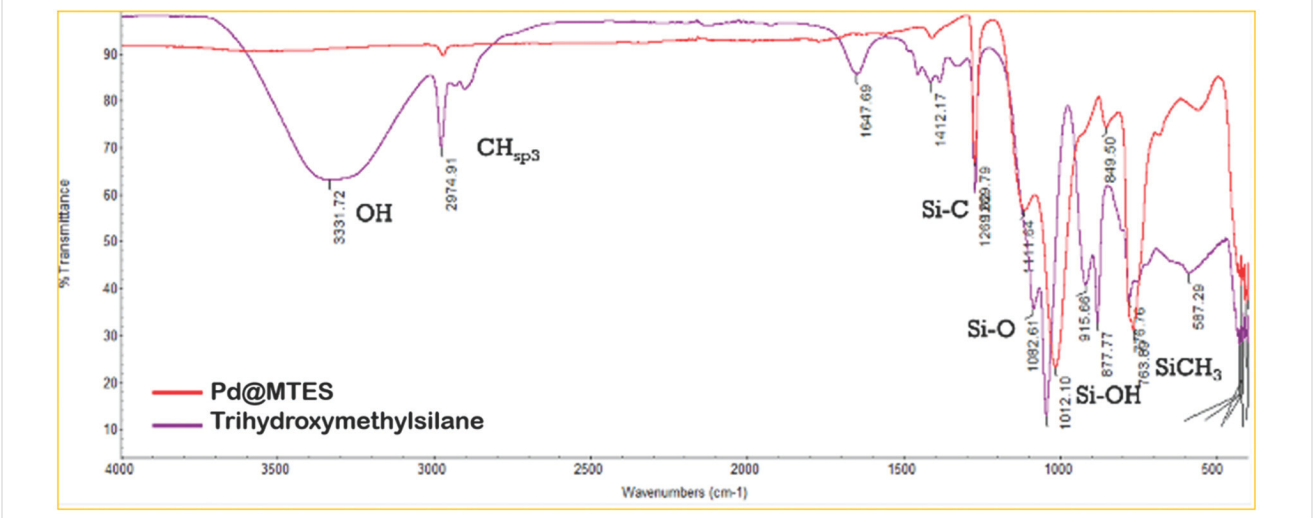

Figure 1 FT-IR spectra of the trihydroxymethylsilane (purple) and the Pd@MTES catalyst (red)

Table 1 Comparative FTIR Data for the Sol-Gel Catalyst (Pd@MTES) and That of Hydrolyzed and Non-polymerized Triethoxymethylsilane (MTES)

Signal	Trihydroxymethylsilane	Pd@MTES
ν(O–H) (cm^{-1})	3331.72	–
νCHsp^3 (cm^{-1})	2974.91	2970.03
ν(Si–C) (cm^{-1})	1269.62	1269.79
ν(O–Si–O) (cm^{-1})	1082.61 1042.10	1111.64 1012.10
ν(Si–OH) bending (cm^{-1})	915.64	–
ν[(Si)CH_3] bending (cm^{-1})	776.76	763.89

The distribution of metal nanoparticles within this material was analyzed by transmission electron microscopy (TEM), while the surface morphology was explored using scanning electron microscopy (SEM). TEM indicated that the particles are generally of a small size, with a diameter of approximately 2–5 nm, and uniformly distributed within the siloxane network, as shown in Figure 2.

The SEM image (Figure 3a) of Pd@MTES indicates that the morphology of the surface of the catalyst is rough and granular. A further study of the surface composition using X-ray photoelectron spectroscopy (XPS) revealed signals corresponding to silicon (Si 2p), carbon (C 1s), oxygen (O 1s), and palladium (Pd 3d) in the survey scan (Figure 3b), with binding energies of around 102.67, 284.92, 532.12, and 335.02 eV, respectively. The deconvolution of the Si(2p) signal revealed superimposed peaks at 102.45 (Si 2p3/2) and 102.79 (Si 2p1/2) eV (Figure 3c), characteristic of silicones and siloxanes.[32]

The C 1s XPS emission for the CH_3–Si region of the silicate matrix displayed two signals fitted to C–Si and C–O at 284.8 and 288.22 eV (Figure 3d), respectively.[33] While the C–Si bond is an inextricable and expected part of the siloxane network,[12] the C–O can be attributed to the residual and uncleaved ethoxy groups from methyltriethoxysilane, used in the sol-gel preparation.

The preponderance of these data, added to the deconvoluted peaks of O (1s) at 532.33, 531.58, and 536.48 eV (Figure 3e) suggest that the surface of the catalyst is primarily composed of organically modified silicate materials. It is important to note, however, that the same XPS surface analysis for Pd (3d) shows two main peaks at binding energies of 335.02 and 340.29 eV assigned to Pd 3d5/2 and Pd 3d3/2 (Figure 3f), respectively, suggesting the presence of metallic Pd(0).[34] Two additional peaks with much lower intensity at binding energies of 334.93 and 341.61 eV were indexed to Pd 3d5/2 and Pd 3d3/2, respectively, suggesting the probable presence of Pd(II) species.[34] Nevertheless, Pd(0) appears to be the major palladium species (68.2%) on the surface of the catalyst based on integration areas, with the overall palladium load estimated at 3.3% of the material by weight.

With the catalyst prepared and fully characterized, its exploration as a potential catalyst for the hydrosilylation of aldehydes and ketones could begin. The initial conditions for this study were carried over from a previous report in our lab, which dealt with the hydrosilylation of olefins using Pt@MTES as a catalyst in toluene as a solvent.[5] A quick optimization of the reaction conditions was undertaken, using *p*-tolualdehyde and triethylsilane as starting materials, as illustrated in Scheme 1, with the data obtained from the evaluated conditions presented in Table 2.

Scheme 1 Hydrosilylation of *p*-tolualdehyde by triethylsilane in the presence of Pd@MTES

While only a 23% yield was observed with 1 mol% of Pd@MTES at room temperature for 18 hours in toluene (Table 2, entry 1), the yield improved to 35% when the temperature was raised to 60 °C (entry 2). Increasing the amount of triethylsilane from 1 equivalent to 1.5, in relation to the number of moles of *p*-tolualdehyde (entry 3), resulted in a modest improvement, with the reaction reaching

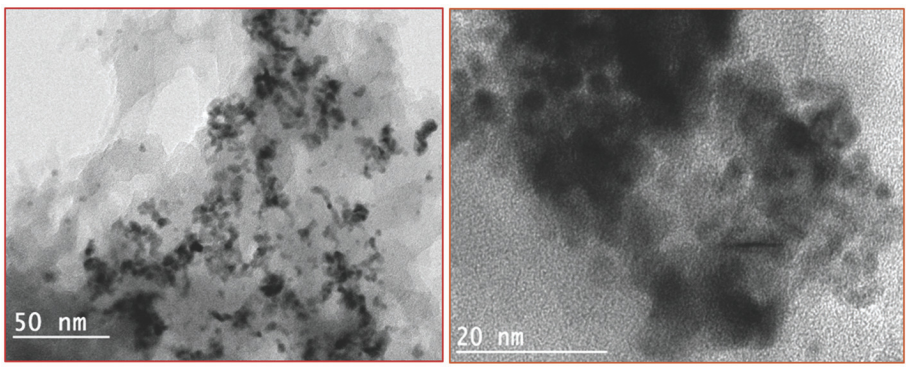

Figure 2 TEM micrographs of Pd@MTES

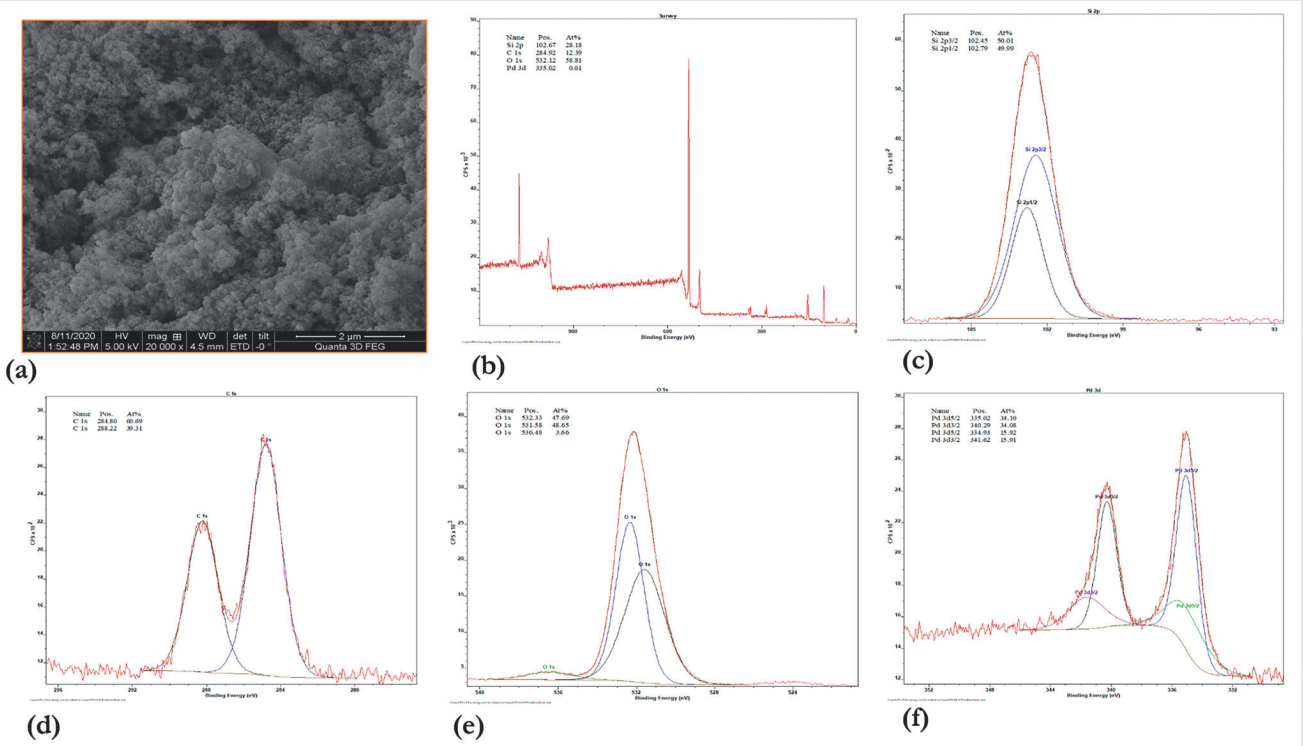

Figure 3 (a) SEM image, (b) XPS scan survey, (c) Si(2p) XPS spectrum, (d) C(1s) XPS spectrum, (e) O(1s) XPS spectrum, and (f) Pd(3d) XPS spectrum of Pd@MTES

completion when heated at 90 °C for 18 hours in toluene (entry 4). However, reducing the reaction time to 6 hours negatively impacted the reactions (entry 5), with an increase in the amount of triethylsilane to 2 equivalents (entry 6) or the catalyst load to 2 mol% (entry 7) failing to have any significant impact on the reaction outcome.

The use of other solvents, including isopropanol, THF, or dioxane (Table 2, entries 8, 9, and 10, respectively), negatively impacted the reaction outcome. Strikingly, this reaction appeared to reach completion under neat conditions at 90 °C in the presence of 1.5 equivalents of triethylsilane and 1 mol% catalyst load (entry 11). However, reducing the temperature to 60 °C (entry 12) or the catalyst load by half (entry 13) under the latest conditions appeared to negatively impact the reaction. It should be mentioned that no reaction was observed in the total absence of a catalyst, with only the starting materials present in the reaction mixture at the end, as indicated by GC-MS (entry 14). As a result, the conditions shown in entry 11 were selected for a further exploration of the reaction scope. The presence of the disilane byproduct resulting from homocoupling of the silane starting material in each of the reaction mixtures also indicates that the use of an excess of silane is necessary for optimal reaction conditions.

Table 2 Exploration of the Reaction Conditions Using *p*-Tolualdehyde and Triethylsilane[a]

Entry	$HSiEt_3$ (equiv)[a]	Pt@MTES (mol%)[b]	Solvent (1 M)	Temp (°C)	Time (h)	Yield (%)[c]
1	1.0	1.0	toluene	rt	18	23[d]
2	1.0	1.0	toluene	60	18	35[d]
3	1.5	1.0	toluene	60	18	46[d]
4	1.5	1.0	toluene	90	18	97
5	1.5	1.0	toluene	90	6	69[d]
6	2.0	1.0	toluene	90	6	70[d]
7	1.5	2.0	toluene	90	6	73[d]
8	1.5	1.0	iPrOH	reflux	18	67[d]
9	1.5	1.0	THF	reflux	18	55[d]
10	1.5	1.0	dioxane	90	18	65[d]
11	**1.5**	**1.0**	**neat**	**90**	**18**	**98**
12	1.5	1.0	neat	60	18	67[d]
13	1.5	0.5	neat	90	18	42[d]
14	1.5	none	neat	90	18	NR[e]

[a] Reactions were performed under a nitrogen atmosphere, using 100 mg of *p*-tolualdehyde.
[b] In relationship to the number of moles of *p*-tolualdehyde.
[c] Percent yields determined by GC-MS, using tridecane as an internal standard.
[d] The reactions did not go to completion, as indicated by GC-MS.
[e] NR = no reaction.

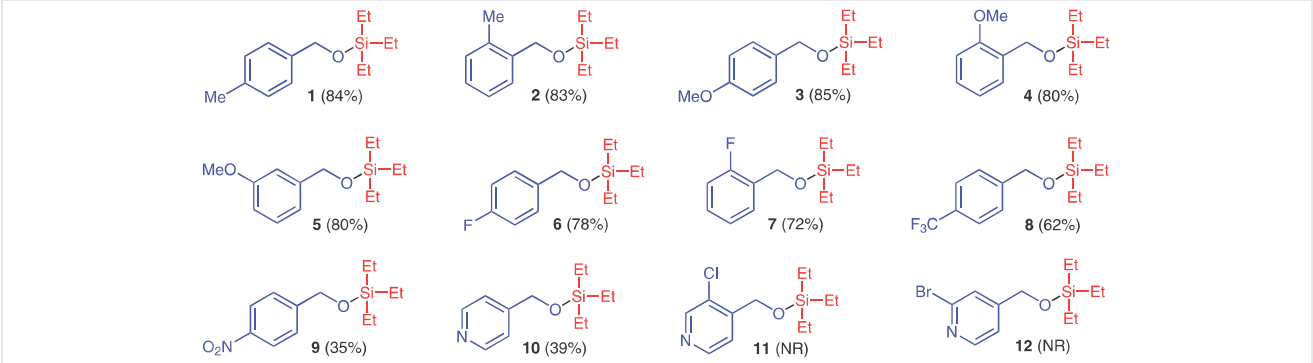

Figure 4 Exploration of the hydrosilylation of activated and deactivated aromatic aldehydes using triethylsilane. Isolated yields are given; NR = no reaction, as only the starting material was observed in the GC-MS spectrum of the reaction mixture.

In order to evaluate the electronic effects of diverse groups on this reaction, priority was given to substituted benzaldehydes, which were seamlessly transformed into their corresponding *O*-silylbenzyl derivatives under the optimal reaction conditions, as illustrated in Figure 4.

This reaction works well with activated systems, regardless of the position of the electron-donating group on the core benzaldehyde structure (Figure 4). In fact, reactions involving a methyl group at the *para*- (**1**) or *ortho*- (**2**) positions on the benzaldehyde structure produced very good yields, similar to those observed for reactions with a methoxy group at similar positions (**3** and **4**, respectively). Even the reaction involving *meta*-anisaldehyde produced product **5** in an 80% yield. However, the yield of the reaction gradually decreased as the benzaldehyde ring became increasingly deactivated, with reactions involving a fluoro group at the *para*- (**6**) or *ortho*- (**7**) positions producing about 78% and 72% yields, respectively. The reactions involving 4-trifluoromethylbenzaldehyde (**8**: 62%), pyridine-4-carbaldehyde (**10**: 39%), or 4-nitrobenzaldehyde (**9**: 35%), all deactivated systems, produced much lower yields when compared to benzaldehyde derivatives bearing electron-donating groups, with the increase in deactivation inducing a decrease in the obtained yield. However, the reaction systematically failed to produce the corresponding products **11** and **12** with either 3-chloroisonicotinaldehyde or 2-bromoisonicotinaldehyde respectively, with the starting material being recovered at the end of each of these reactions, as indicated by GC-MS analysis of the respective reaction mixtures.

This reaction also works well with several other hydrosilanes, including diethylsilane, methyldiethoxysilane, triisopropylsilane, and benzyldimethylsilane, as illustrated in Figure 5. This catalytic system produced similar yields with diethylsilane as it did with triethylsilane when involving *para*- or *ortho*-tolualdehyde, as well as *para*- or *ortho*-ani-

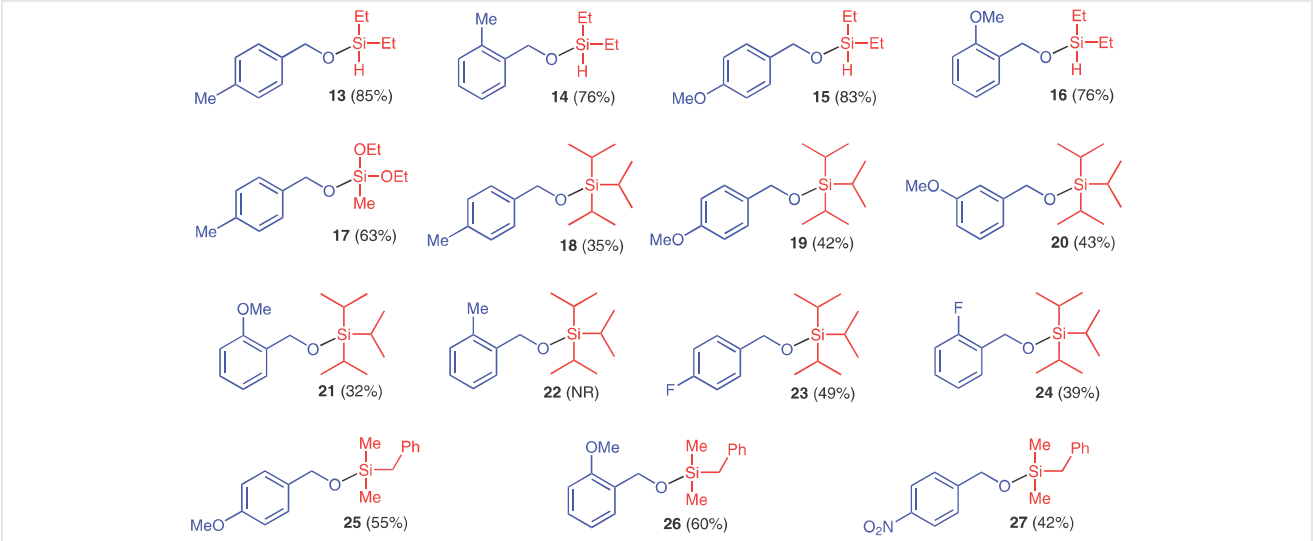

Figure 5 Exploration of the hydrosilylation of activated and deactivated benzaldehydes using other hydrosilanes. Isolated yields are given; NR = no reaction, as only the starting material was observed in the GC-MS spectrum of the reaction mixture.

saldehyde as starting materials, as shown with products **13** to **16**, respectively. It should also be mentioned that many substrates produced the corresponding hydrosilylated products with methyldiethoxysilane, but only compound **17** was purified and fully characterized. The other products obtained from methyldiethoxysilane systematically decomposed during the purification process, regardless of whether silica or alumina neutral gel was used for chromatography, with the hydrosilane being cleaved every single time. In fact, none of the products described in this report could survive purification on silica gel, and as a result, alumina neutral gel was used for chromatography, with the Combi-Flash apparatus enabling each compound to exit the column in no more than 10 minutes.

The yield of the reaction decreased significantly when bulky silanes, such as triisopropylsilane (compounds **18** to **24**) or benzyldimethylsilane (**25** to **27**), were used as reagents (Figure 5). In fact, this reaction could not produce an isolated yield greater than 50% when triisopropylsilane was used, and was also unable to produce any product with a combination of triisopropylsilane and *o*-tolualdehyde, even after several trials. It is conceivable that this failure might be due to extreme steric issues resulting from the methyl group being at the *ortho*-position to the reaction center on the benzaldehyde. Consequently, it was concluded that the only reason *o*-anisaldehyde was able to produce some product **21** might be related to the fact that the oxygen atom of the methoxy group angles the bulky methyl away from the reaction center, allowing the process to proceed to a certain extent. Furthermore, with triisopropylsilane as the reagent, there was no real difference between activated (compounds **18**–**22**) and deactivated (compounds **23** and **24**) benzaldehydes. In addition, the yield of the reaction improved when benzyldimethylsilane was used as the silylating agent, as illustrated with compounds **25** to **27** in Figure 5.

The scope of the reaction was rather limited as far as ketones are concerned. Acetophenone (**28**) produced only a low yield, while activated 2′-methoxyacetophenone (**29**) yielded a decent result, as shown in Figure 6. The steric hindrance generated by the methyl group of acetophenone is likely to blame for the low yield in these cases. The situation worsened when a deactivated system, including 4′-chloroacetophenone and 4′-bromoacetophenone (not shown), or 4′-nitroacetophenone (**32**), was used as a substrate. In each of these cases, the reaction systematically failed, and the starting material was recovered each time, as indicated by the GC-MS spectrum of each reaction mixture. The reaction also failed to produce any product when 4′-iodo-2′-methoxyacetophenone (**31**), which carries a deactivator at the *para*-position and an activator at the *ortho*-position, was used, with the starting material recovered at the end of the reaction. A similar outcome was observed with any of the benzophenone derivatives explored during this study, as illustrated with compounds **33**, **34**, and **35** (Figure 6). The steric hindrance created by the two benzene rings of the benzophenones likely precluded the reaction from proceeding. Additionally, some deactivated benzophenones (not shown) were also explored under the optimal reaction conditions, and each of these substrates failed to produce the expected product, with the starting material recovered each time.

The reusability of the catalyst was explored using *p*-tolualdehyde and triethylsilane as reagents in the preparation of compound **1** under the optimized conditions (see entry 11 in Table 2). The catalyst was recovered from the reaction mixtures by centrifugation, followed by removal of the supernatant through decantation at the end of each cycle. Each catalyst was then sonicated for about 45 minutes in THF, washed, and air-dried before the next run. To compensate for the catalyst loss during each recovery, the amount of substrate was adjusted for each cycle. The percentage yields were determined by GC-MS using tridecane as an internal standard, in a similar fashion to the study in Table 2.

The obtained results (Figure 7) indicate about a 14% decrease in yield from the first run to the second, about 7% from the second to the third, and about a 12% drop in yield from the third to the fourth cycle. After the fourth run, the amount of the recovered catalyst became too small to be used for another cycle. The decrease in yield appeared to be primarily associated with blockage of the pores in the sol-gel material, rather than a loss of catalytic activity. In fact, the reduction in yield appeared to be more dramatic when the catalyst was not sonicated between cycles. It is note-

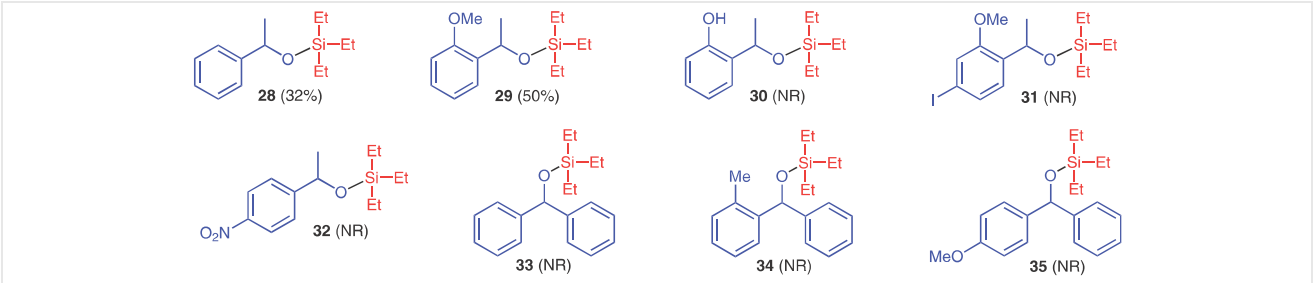

Figure 6 Exploration of the hydrosilylation of ketones. Isolated yields are given; NR = no reaction, as only the starting material was observed in the GC-MS spectrum of the reaction mixture.

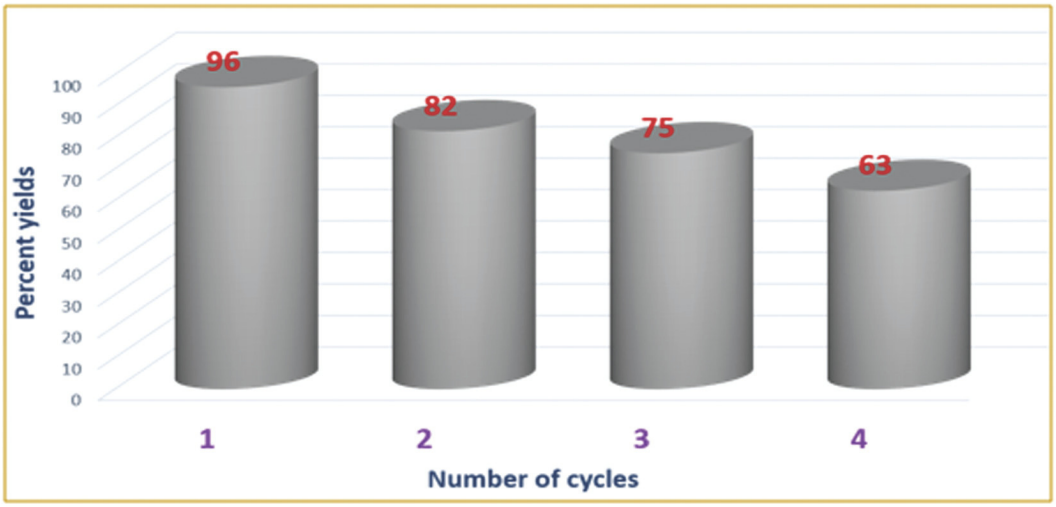

Figure 7 A study of the reusability of Pd@MTES, using *p*-tolualdehyde and triethylsilane as reagents for the preparation of **1**. The percentage yields were determined by GC-MS, using tridecane as an internal standard.

worthy to mention that this catalyst showed no sign of leaching when repeatedly heated for 18 hours in either THF or toluene, as observed by analyzing the different filtrates by atomic absorption spectroscopy and atomic emission spectroscopy.

While the catalytic cycle for the Pd-catalyzed hydrosilylation process in homogeneous catalysis is well-documented,[24,35] the reactions described in this report proceed primarily through heterogeneous or surface catalysis. As such, it is anticipated that both starting materials are absorbed on the surface of the catalyst, enabling splitting of the Si–H bond. This process allows the H* atom to attach to the carbon, while the Si* group binds to the oxygen side of the C=O through rupture of the π-bond. This process can occur via two possible paths: path 1, in which the H* atom attaches first to the carbon of the carbonyl group followed by the Si* group linkage to the other side, or path 2, in which the Si* group binds first to the oxygen of the carbonyl group, followed by the attachment of the H* atom to the carbon on the other side of the π-bond.

In order to determine which path is kinetically favorable, DFT calculations were used to construct the free energy profiles for the two possible mechanistic pathways on the Pd(111) surface, with the hydrosilylation of benzaldehyde by trimethylsilane used as a simplified model for the calculations, as illustrated in Scheme 2.

In path 1, C–H bond formation to the adsorbed benzaldehyde occurs first in step 1a, leading to intermediate **I1**, followed by O–Si bond formation in step 1b to yield the adsorbed product. Conversely, in path 2, O–Si bond formation occurs first in step 2a resulting in intermediate **I2**, followed by C–H bond formation to yield the adsorbed product

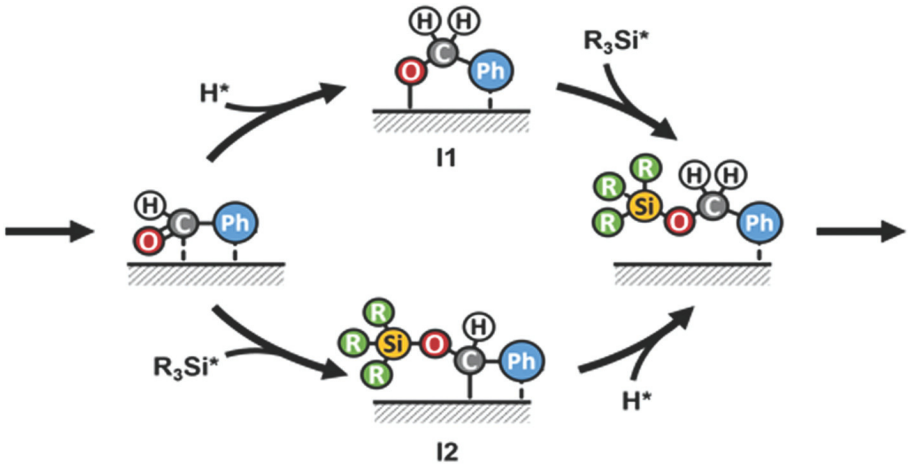

Scheme 2 Mechanistic pathways for the hydrosilylation of benzaldehyde used as a simplified model for calculations

(Scheme 2). The kinetic analysis was also based on the assumption that the dissociation of trimethylsilane is quasi-equilibrated and therefore not kinetically relevant.

The lowest free energy state of the surface in the presence of 1 mol/L of both reactants and the product at the reaction temperature of 90 °C was determined and used as the starting point. Benzaldehyde and the product are both expected to adsorb molecularly on the surface through interactions involving the π-system and dispersion. This adsorption on the clean surface proved to be associated with a decrease in free energy of –0.23 eV for benzaldehyde and –0.50 eV for the product. For both species, the benzene ring adsorbs onto an ensemble of four Pd atoms, as depicted in Figure 8, which has been shown in previous DFT studies to be the most favorable adsorption site on Pt(111).[36] The carbonyl group in benzaldehyde and the oxygen in the product additionally interact with a fifth Pd atom. The maximum coverage of benzaldehyde is estimated to be around 1/9 of a monolayer, while the maximum coverage of the product is 1/12 of a monolayer due to its larger size. Structures of saturated adlayers are shown for both species in Figure S1 in the Supporting Information. At these higher coverages, the adsorption free energy of benzaldehyde actually decreases to –0.49 eV due to attractive lateral interactions in the adlayer, presumably dominated by dispersion, while the adsorption free energy of the product increases to –0.41 eV due to repulsive lateral interactions.

Trimethylsilane adsorbs by dissociating into atomic H* and a trimethylsilyl fragment (Me_3Si^*), with H* sitting in a 3-fold site and Me_3Si^* on an atop site as depicted in Figure 8. The free energy for dissociative adsorption is –0.64 eV on the clean surface when the Me_3Si^* and H* fragments are infinitely separated. It was estimated that the maximum coverage of a mixed Me_3Si^*/H* adlayer is around 1/8 of a monolayer, with the corresponding structure of the adlayer shown in Figure S1 in the Supporting Information. At this higher coverage, the adsorption free energy decreases to –0.58 eV due to repulsive lateral interactions in the adlayer.

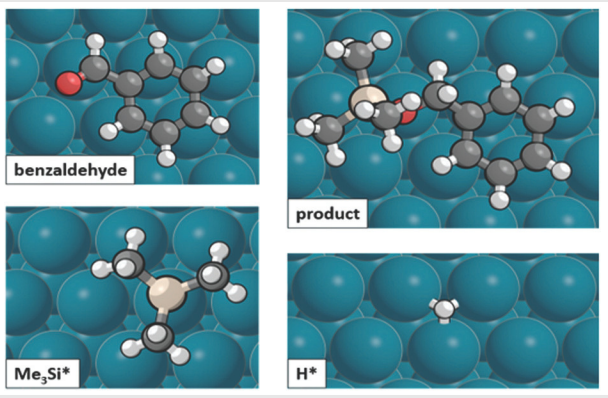

Figure 8 Structures of benzaldehyde, the product, Me_3Si^*, and H* on the Pd(111) surface

Ab initio thermodynamics[37] can be used to determine the most favorable adsorbate coverage in the resting state of the catalyst surface under the reaction conditions. The results (presented in Figure S1 in the Supporting Information) indicate that the surface with 1/8 ML of Me_3Si^*/H* has the lowest free energy normalized to the number of surface atoms, with a free energy of –0.070 eV/Pd. Therefore, the Me_3Si^*/H* covered surface was used as the initial resting state for the catalytic cycle. Furthermore, for benzaldehyde to adsorb on the surface, it is necessary to remove one or more molecules of trimethylsilane in order to make room for it, resulting in a free energy penalty of 0.64 eV for each molecule removed. The number of molecules of trimethylsilane to be removed was determined based on the estimated surface area occupied by adsorbed benzaldehyde. This method is detailed in the Supporting Information and is based on the projection of the Connolly surface of the adsorbate onto the plane of the metal surface. Using this approach, 1.35 molecules of trimethylsilane must desorb in order for benzaldehyde to adsorb, leading to a free energy penalty of 0.76 eV and a net adsorption free energy of 0.53 eV. This procedure is used to compute the displacement penalty for all intermediates and transition states.

The calculated transition state structures for the four steps 1a, 1b, 2a, and 2b are depicted in Figure 9, along with the structures of the two intermediates **I1** and **I2**. The formation of the C–H bond in step 1a proceeds via the transition state **TS1a**, reminiscent of hydride transfer to a carbonyl group, whereby the H atom is in transit between a Pd atom and C1 while the O atom is in the process of forming a bond with a second Pd atom. The Pd–H and C–H bond distances in **TS1a** were determined to be 1.66 and 1.57 Å, respectively, while the C–O and Pd–O bond distances were 1.28 and 2.21 Å. The intrinsic activation free energy with respect to infinitely separated benzaldehyde and H* was found to be 1.11 eV, and the overall reaction appeared to be uphill in free energy by 0.69 eV. The resulting intermediate **I1** displayed C–O and Pd–O bond distances of 1.40 and 2.02 Å, respectively.

In the transition state for step 1b (**TS1b**), the Si and O sit on adjacent Pd sites with a partially formed Si–O bond (Figure 9). As the reaction progresses, the Pd–Si and Pd–O bonds break as the Si–O bond is formed. The lengths of the Pd–Si and Pd–O bonds increase from 2.38 and 2.02 Å in the initial state to 2.50 and 2.09 Å in the transition state, respectively. The Si–O bond in the transition state is 2.21 Å compared to 1.69 Å in the final state. The free energy barrier to form the transition state **TS1b** from **I1** and Me_3Si^* was determined to be 0.41 eV, with the step being significantly downhill in free energy by –1.29 eV.

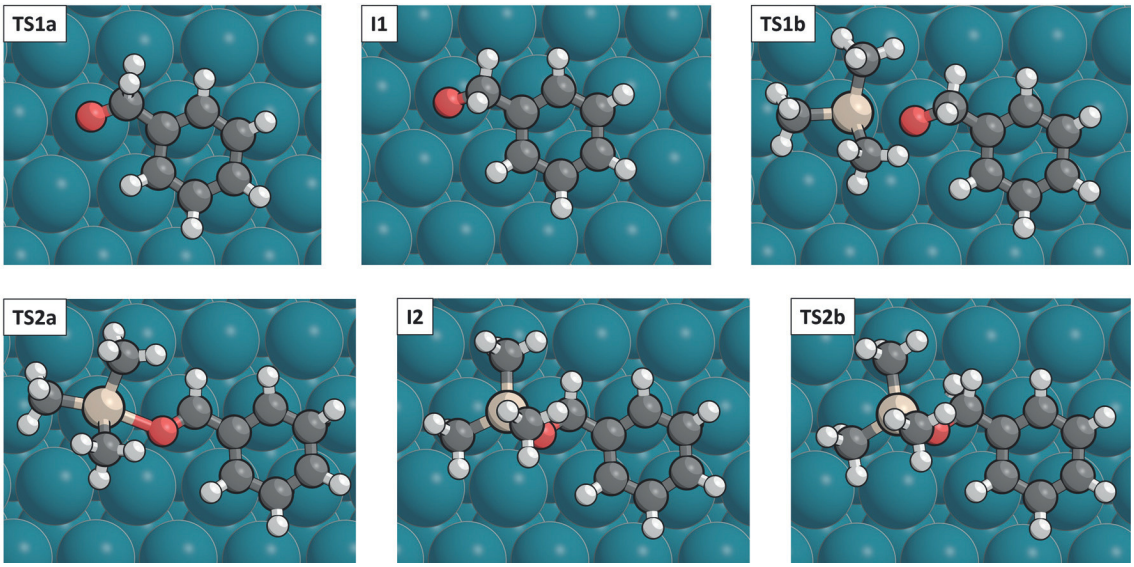

Figure 9 Structures of the transition states and intermediates in path 1 (top) and path 2 (bottom)

The second pathway begins with step 2a proceeding through transition state **TS2a** in which a Si–O bond is formed between Me_3Si^* and the O of adsorbed benzaldehyde (Figure 9). The Si and C1 sit on adjacent Pd sites, with the Pd–Si bond breaking and the Si–O and Pd–C bonds forming as the reaction progresses. The Pd–Si bond lengthens from 2.38 Å in the initial state to 2.54 Å in the transition state, while the Pd–C bond decreases from 2.55 to 2.22 Å. The Si–O bond is 2.16 Å in the transition state and decreases to 1.71 Å in the resulting intermediate **I2**. The C–O bond also increases in length as the reaction progresses, from 1.24 Å in the initial state to 1.30 Å in the transition state and 1.36 Å in the final state. The C1 atom in the final state (**I2**) exhibits significant π-bonding with the oxygen atom and the C2 atom in the adjacent ring, evidenced by shortened C–O and C–C bond distances of 1.36 and 1.47 Å, respectively. The free energy barrier between **TS2a** and adsorbed benzaldehyde on the Me_3Si^*/H^* covered surface appeared to be 0.67 eV, and the step is significantly downhill in free energy by –0.83 eV.

The transition state for C–H bond formation in step 2b also resembles a hydride transfer process, whereby the bond between C1 and the surface breaks prior to formation of the C–H bond. The H atom sits in a Pd_2 bridge site in the transition state with a C–H bond distance of 1.62 Å. The C1 atom exhibits a similar degree of π-bonding with the O and C2 atoms in **TS2b** as in **I2**, with nearly identical bond distances of 1.35 and 1.47 Å, respectively (Figure 9). In the final state, these bonds both lengthen to 1.42 and 1.52 Å due to loss of the π-interaction upon completion of the C–H bond formation. The free energy barrier to reach **TS2b** from **I2** and adsorbed Me_3Si^* was determined to be 0.95 eV, and the step is uphill in free energy by 0.24 eV.

The free energy profile for both pathways is depicted in Figure 10, along with a second set of profiles depicting the resting free energy profile. The resting free energy profile is calculated based on the surface coverages of each intermediate or transition state under actual steady-state conditions, rather than the standard state condition of saturated surface coverage. Plaisance and Khezeli introduced this quantity in a previous work, showing that it can be used to determine the reversibility and degree of rate control of each step as well as for identifying the resting state from which each step proceeds.[38]

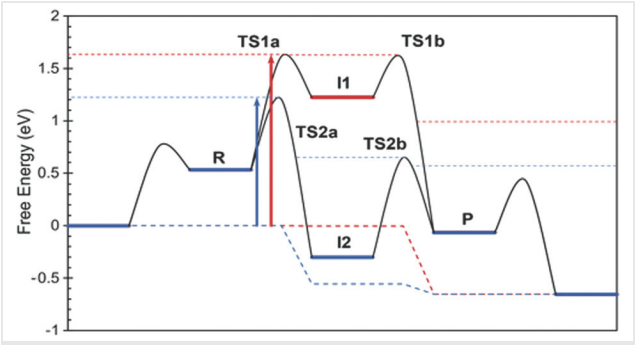

Figure 10 Free energy profiles for path 1 (red) and path 2 (blue). The dashed lines indicate the resting free energy profiles and the arrows indicate the total barrier of the rate-limiting step for each path.

Looking at the free energy profile, it can be seen that the Me_3Si^*/H^* covered surface is the resting state for both steps of path 1. Step 1a is reversible since **I1** is higher in free energy than the Me_3Si^*/H^* covered surface, while step 1b is irreversible. Both steps are rate-limiting with almost identical total barriers of 1.64 eV and 1.63 eV, respectively. For path

2, step 2a proceeds from the initial resting state and is rate-limiting and irreversible with a total barrier of 1.20 eV, and step 2b is also irreversible and proceeds from the resting state **I2** with a total barrier of 0.95 eV. Overall, it can be concluded that path 2 is the dominant hydrosilylation pathway since the total barrier of its rate-limiting step (1.20 eV) is significantly lower than that of path 1 (1.64 eV). This pathway is favored because intermediate **I2** has significantly lower free energy than intermediate **I1** involved in path 1 (Figure 10).

These calculations also suggest that the reaction should be first order with respect to the aldehyde and negative order with respect to the silane as the surface is covered by the latter. This implies that the rate of the reaction could be significantly improved if the silane concentration were kept low, probably through gradual addition using a syringe pump. The calculations also suggest that bulkier aldehydes should be less reactive since they occupy more surface area and thus require the desorption of more silane in order to adsorb, while electron-donating substituents should make them more reactive since **TS2a** and **TS2b** both appear to have cationic character on the C1 position. In contrast, electron-withdrawing substituents should make them less reactive. These latter predictions are in full agreement with the experimental data as described above.

In conclusion, a heterogeneous catalytic system for the hydrosilylation of aldehydes and ketones involving palladium nanoparticles dispersed and stabilized in organically modified silicate (Pd@MTES) as a catalyst has been developed. The reaction conditions were optimized and the scope of the reaction explored. This catalyst, prepared and fully characterized in our laboratory, produced better yields with electron-rich systems compared to the reduced yields observed with electron-poor systems. The reaction also yielded lower yields with either bulky aldehydes or bulky silanes, with many ketones failing to produce any product.

A proposed mechanism suggested two possible pathways for the reaction, with DFT calculations indicating that the pathway involving the formation of the O–Si bond prior to that of the C–H bond (path 2) is energetically favored over that proceeding via the formation of a C–H bond in the first step, followed by O–Si bond formation in the second (path 1). Overall, this work provides a unique insight into the catalytic effect of palladium nano-dispersed and stabilized in silicate sol-gel toward the hydrosilylation of aldehydes and ketones.

All chemicals and solvents were purchased from major chemical suppliers and were used without further purification unless stated otherwise. NMR data were collected on a Bruker Ascend™ 400 spectrometer operating at 400 MHz for ^{1}H and 100 MHz for ^{13}C. The concentration of each sample was approximately 20 mg in 0.5 mL of $CDCl_3$. The NMR data were recorded at 300 K, with chemical shifts (δ) reported in parts per million (ppm) relative to TMS (δ_H 0.00 and δ_C 0.0) used as the internal standard, or residual chloroform (δ_H 7.28 and δ_C 77.2), and coupling constants (*J*) in hertz. The multiplicity for each signal is listed as follows: s = singlet, d = doublet, t = triplet, q = quartet, quin = quintet, m = multiplet. Structures were confirmed based on NMR data including proton and broadband carbon 13. The IR experiments were performed on a Nicolet iS20 FTIR spectrometer. XPS measurements were performed using a ScientaOmicron ESCA 2SR X-ray photoelectron spectroscope system equipped with a flood source charge neutralizer. The powder samples were pressed into a little pellet and fixed on the sample stage with double-sided carbon tape. Samples were loaded into the load lock and pumped until the vacuum was below 5×10^{-7} mbar, before they were transferred into the sample analysis chamber. All analyses were conducted with a mono Al Kα X-ray source (1486.6 eV) at a power of 450 W, whilst the pressure in the analysis chamber was maintained below 3×10^{-9} mbar. A wide region survey scan and high-resolution core level scans of all elements were recorded and calibrated with C1s 284.8 eV as the reference peak. The core level spectra were deconvoluted to obtain information on the chemical state. SEM imaging and EDS analysis was conducted with a FEI Quanta 3D FEG FIB/SEM dual-beam system interfaced with an EDAX Apollo XL EDS detector. The powder samples were fixed on the SEM stub with double-sided carbon tape and then coated with a thin layer of Pt to avoid the charging effect during imaging and analysis. The TEM imaging data are acquired on a JEOL 2011 TEM operated at 200 kV. TEM samples were prepared following the standard protocol: grinding, mixing with ethanol into a suspension, ultrasonic bathing, vortexing and applying to a holey carbon film supported by 300 mesh Cu grids.

Computational Details

A free energy profile was constructed to visualize the kinetics of the elementary steps and the overall catalytic cycle. Full details of the DFT calculations carried out to construct this profile are given in the Supporting Information. These calculations were performed using the Vienna Ab initio Simulation Package (VASP),[39] employing the Bayesian error estimation functional with van der Waals correlation (BEEF-vdW).[40] Transition states were found by performing a roughly converged nudged elastic band calculation[41] to obtain an initial guess, followed by a dimer calculation[42] to refine the transition state.

The free energies of intermediates and transition states were determined by adding vibrational contributions and a site coverage penalty to the electronic energy E_0 computed by VASP,

$$(1)\ G^\circ = E_0 + E_{ZPVE} + G_{vib} - n_S\mu_S$$

where E_{ZPVE} is the zero-point vibrational energy and G_{vib} is the vibrational free energy in the harmonic approximation, both computed from a vibrational frequency calculation on the optimized structure. A temperature of 90 °C was used for all free energy calculations. The site coverage penalty implicitly accounts for the free energy penalty to adsorb a species on a surface that is already covered with another species A. In order to place a species on the surface that occupies n_S metal sites, a number $n_S/n_{S,A}$ of species A must first desorb from the surface where $n_{S,A}$ is the number of metal sites occupied by species A. If the free energy of species A to desorb from the surface is $-\Delta G_A^{ads}$, then the desorption penalty is $-n_S\mu_S$, where $\mu_S = \Delta G_A^{ads}/n_{S,A}$ represents the effective chemical potential of a metal site. The free energies of the reactants and products in the liquid phase are computed by,

$$(2)\ G^\circ = E_0 + E_{ZPVE} + G^\circ_{trans} + G_{rot} + G_{vib}$$

where G°_{trans} is the translational free energy at a concentration of 1 mol/L and G_{rot} is the rotational free energy in the rigid rotor approximation. The Pd catalyst is modeled as a periodic Pd(111) surface consisting of four layers each containing a 6 × 4 surface unit cell. The ex-

perimental lattice constant of 3.89 Å was used for the fcc unit cell from which the surface was cut, and the slabs were separated by 20 Å of vacuum. The bottom two layers of the slab were frozen during geometry optimization, while all other atoms were allowed to relax. Calculations of the reactants and products in the liquid phase were performed in a 20 × 20 × 20 $Å^3$ unit cell.

Palladium(0) Nano-Dispersed in Organically Modified Silicate (Pd@MTES)

The general protocol for the preparation of Pd@MTES was based on a modified version of previously reported methods,[5,9] and consisted of stirring vigorously methyltriethoxysilane (MTES) (27 g, 30 mL, 151.4 mmol) in about 10 mL of 0.05 M HCl until the solution became homogeneous. Next, a solution of palladium nitrate dihydrate ($Pd(NO_3)_2{\cdot}2H_2O$) (3 g, 0.113 mmol, 0.074 equiv) dissolved in 15 mL of H_2O was added, and the mixture was stirred until a brownish homogeneous solution was obtained. About 22 mL of 1 M NaOH (0.05 equiv) was added to the mixture until the solution became basic, as indicated by pH paper (pH ~ 8), and the mixture was then stirred until gelation occurred. The resulting homogeneous and transparent gel was allowed to air dry for 4 days. The dark xerogel obtained was reduced with a solution of sodium borohydride (ratio $Pt/NaBH_4$ = 1:10) in 50 mL of THF/H_2O (1:1), and the resulting material was washed with distilled water (2 × 100 mL) and THF (100 mL), and air-dried at room temperature. This provided Pd@MTES that was ready to be used. The distribution of metal nanoparticles within this material was analyzed by transition electron microscopy (TEM), while the morphology of the surfaces was explored by scanning electron microscopy (SEM). Qualitative and quantitative chemical microanalysis of this material was achieved using X-ray photoelectron spectroscopy (XPS), which enabled an accurate determination of the metal content as well as its chemical state.

Hydrosilylation of Aldehydes and Ketones

Most reactions were set up using 200 mg of the carbonyl-containing starting material (aldehyde or ketone), 1.5 equiv of the appropriate silane, and 1 mol% of Pd@MTES under a nitrogen-saturated environment for 18 h. All the reactions were run under neat conditions, except for those of some solid starting materials for which 500 µL of toluene was added to enable effective stirring. Reaction mixtures were monitored using a 200-MS GC-MS ion trap mass spectrometer or by TLC on silica gel 60 F254 plates. All purifications were performed on a Teledyne Isco CombiFlash Rf, using pre-packed alumina neutral columns (surface area 14–170 m^2/g, pore diameter 50–70 Å, particle size 50–75 µm), namely REDISepRF (48 g) from Teledyne Isco, or FlashPure EcoFlex (50 g) from Buchi Corporation. Each purification was achieved under gradient elution, using mixtures of hexane and ethyl acetate.

Triethyl(4-methylbenzyloxy)silane (1)[24,43]

p-Tolualdehyde (200 mg, 1.66 mmol) and triethylsilane (290 mg, 2.50 mmol) were stirred in the presence of 1 mol% of the Pd@MTES catalyst (having ca. 3.3% palladium content) (53.7 mg, $1.66{\cdot}10^{-5}$ mol) under neat conditions and a nitrogen environment for 18 h. The reaction mixture was then purified on a CombiFlash apparatus, on a neutral alumina prepacked column, using a gradient elution from pure hexane to a mixture of hexane/ethyl acetate (9:1). The product eluted after 7.30 minutes as a clear oil (331 mg, 84%).

^{1}H NMR (400 MHz, $CDCl_3$): δ = 0.65 (q, *J* = 7.2 Hz, 6 H), 0.97 (t, *J* = 7.2 Hz, 9 H), 2.31 (s, 3 H), 4.68 (s, 2 H), 7.11 (d, *J* = 6.2 Hz, 2 H), 7.20 (d, *J* = 6.2 Hz, 2 H).

^{13}C NMR (100 MHz, $CDCl_3$): δ = 3.6, 5.8, 20.1, 63.6, 125.3, 127.9, 135.5, 137.3.

GC-MS: *m*/*z* (%) = 237 (1) $[M + H]^+$, 219 (33), 207 (100), 105 (69).

Triethyl(2-methylbenzyloxy)silane (2)[44]

o-Tolualdehyde (200 mg, 1.66 mmol) and triethylsilane (290 mg, 2.50 mmol) were stirred in the presence of 1 mol% of the Pd@MTES catalyst (having ca. 3.3% palladium content) (53.7 mg, $1.66{\cdot}10^{-5}$ mol) under neat conditions and a nitrogen environment for 18 h. The reaction mixture was then purified on a CombiFlash apparatus, on a neutral alumina prepacked column, using a gradient elution from pure hexane to a mixture of hexane/ethyl acetate (9:1). The product eluted after 6.43 minutes as a clear oil (327 mg, 83%).

^{1}H NMR (400 MHz, $CDCl_3$): δ = 0.61 (q, *J* = 7.0 Hz, 6 H), 0.98 (t, *J* = 7.0 Hz, 9 H), 2.25 (s, 3 H), 4.68 (s, 2 H), 7.10 (m, 3 H), 7.40 (d, *J* = 6.4 Hz, 1 H).

^{13}C NMR (100 MHz, $CDCl_3$): δ = 4.7, 6.9, 18.6, 63.1, 125.9, 126.7, 127.0, 129.9, 135.2, 139.2.

GC-MS: *m*/*z* (%) = 235 (7) $[M - H]^+$, 220 (28), 207 (100), 177 (10), 149 (12), 105 (79).

Triethyl(4-methoxybenzyloxy)silane (3)[45,46]

p-Anisaldehyde (200 mg, 1.47 mmol) and triethylsilane (256 mg, 2.20 mmol) were stirred in the presence of 1 mol% of the Pd@MTES catalyst (having ca. 3.3% palladium content) (47.4 mg, $1.47{\cdot}10^{-5}$ mol) under neat conditions and a nitrogen environment for 18 h. The reaction mixture was then purified on a CombiFlash apparatus, on a neutral alumina prepacked column, using a gradient elution from pure hexane to a mixture of hexane/ethyl acetate (9:1). The product eluted after 8.02 minutes as a clear oil (315 mg, 85%).

^{1}H NMR (400 MHz, $CDCl_3$): δ = 0.64 (q, *J* = 7.2 Hz, 6 H), 0.97 (t, *J* = 7.6 Hz, 9 H), 3.77 (s, 3 H), 4.66 (s, 2 H), 6.85 (d, *J* = 6.4 Hz, 2 H), 7.24 (d, *J* = 6.4 Hz, 2 H).

^{13}C NMR (100 MHz, $CDCl_3$): δ = 4.6, 6.8, 55.2, 64.5, 113.7, 127.8, 133.5, 158.8.

GC-MS: *m*/*z* (%) = 252 (5) $[M^+]$, 223 (100), 136 (2), 122 (68).

Triethyl(2-methoxybenzyloxy)silane (4)[47,48]

o-Anisaldehyde (200 mg, 1.47 mmol) and triethylsilane (256 mg, 2.20 mmol) were stirred in the presence of 1 mol% of the Pd@MTES catalyst (having ca. 3.3% palladium content) (47.4 mg, $1.47{\cdot}10^{-5}$ mol) under neat conditions and a nitrogen environment for 18 h. The reaction mixture was then purified on a CombiFlash apparatus, on a neutral alumina prepacked column, using a gradient elution from pure hexane to a mixture of hexane/ethyl acetate (9:1). The product eluted after 8.12 minutes as a clear oil (297 mg, 80%).

^{1}H NMR (400 MHz, $CDCl_3$): δ = 0.66 (q, *J* = 7.2 Hz, 6 H), 0.97 (t, *J* = 6.4 Hz, 9 H), 3.79 (s, 3 H), 4.76 (s, 2 H), 6.80 (d, *J* = 6.8 Hz, 1 H), 6.96 (dd, *J* = 6.8, 6.4 Hz, 1 H), 7.20 (dd, *J* = 6.4, 6.6 Hz, 1 H), 7.49 (d, *J* = 6.6 Hz, 1 H).

^{13}C NMR (100 MHz, $CDCl_3$): δ = 4.6, 6.8, 55.1, 59.8, 109.6, 120.5, 127.0, 127.6, 129.8, 156.1.

GC-MS: *m*/*z* (%) = 251 (1) $[M - H]^+$, 242 (5), 233 (100), 205 (57), 192 (10), 166 (23), 153 (9), 121 (7).

Triethyl(3-methoxybenzyloxy)silane (5)[49]

m-Anisaldehyde (200 mg, 1.47 mmol) and triethylsilane (258 mg, 2.22 mmol) were stirred in the presence of 1 mol% of the Pd@MTES catalyst (having ca. 3.3% palladium content) (47.4 mg, $1.47{\cdot}10^{-5}$ mol)

under neat conditions and a nitrogen environment for 18 h. The reaction mixture was then purified on a CombiFlash apparatus, on a neutral alumina prepacked column, using a gradient elution from pure hexane to a mixture of hexane/ethyl acetate (9:1). The product eluted after 7.30 minutes as a clear oil (297 mg, 80%).

^{1}H NMR (400 MHz, $CDCl_3$): δ = 0.70 (q, *J* = 7.2 Hz, 6 H), 1.09 (t, *J* = 7.2 Hz, 9 H), 3.87 (s, 3 H), 4.81 (s, 2 H), 6.86 (d, *J* = 7.2 Hz, 1 H), 7.00 (m, 2 H), 7.33 (m, 1 H).

^{13}C NMR (100 MHz, $CDCl_3$): δ = 4.6, 6.8, 55.0, 64.6, 111.7, 112.5, 118.4, 129.2, 143.1, 159.8.

GC-MS: *m*/*z* (%) = 252 (2) [M^+], 242 (8), 226 (56), 193 (100), 122 (74), 91 (52).

Triethyl((4-fluorobenzyl)oxy)silane (6)[24,46]

p-Fluorobenzaldehyde (200 mg, 1.61 mmol) and triethylsilane (281 mg, 2.42 mmol) were stirred in the presence of 1 mol% of the Pd@MTES catalyst (having ca. 3.3% palladium content) (52.0 mg, $1.61\cdot10^{-5}$ mol) under neat conditions and a nitrogen environment for 18 h. The reaction mixture was then purified on a CombiFlash apparatus, on a neutral alumina prepacked column, using a gradient elution from pure hexane to a mixture of hexane/ethyl acetate (85:15). The product eluted after 7.53 minutes as a clear oil (302 mg, 78%).

^{1}H NMR (400 MHz, $CDCl_3$): δ = 0.64 (q, *J* = 8.0 Hz, 6 H), 0.97 (t, *J* = 8.0 Hz, 9 H), 4.68 (s, 2 H), 6.99 (dd, J_{H-H} = 8.1, J_{H-F} = 8.7 Hz, 2 H), 7.28 (dd, J_{H-H} = 8.1, J_{H-F} = 5.7 Hz, 2 H).

^{13}C NMR (100 MHz, $CDCl_3$): δ = 4.6, 6.8, 64.2, 115.1 (d, $^2J_{C-F}$ = 21.2 Hz), 127.9 (d, $^3J_{C-F}$ = 8.0 Hz), 137.2 (d, $^4J_{C-F}$ = 3.0 Hz), 162.1 (d, $^1J_{C-F}$ = 242.9 Hz).

GC-MS: *m*/*z* (%) = 239 (2) [M – H]$^+$, 220 (5), 211 (37), 183 (68), 154 (44), 105 (100), 86 (69).

Triethyl((2-fluorobenzyl)oxy)silane (7)[46,50]

o-Fluorobenzaldehyde (200 mg, 1.61 mmol) and triethylsilane (281 mg, 2.42 mmol) were stirred in the presence of 1 mol% of the Pd@MTES catalyst (having ca. 3.3% palladium content) (52.0 mg, $1.61\cdot10^{-5}$ mol) under neat conditions and a nitrogen environment for 18 h. The reaction mixture was then purified on a CombiFlash apparatus, on a neutral alumina prepacked column, using a gradient elution from pure hexane to a mixture of hexane/ethyl acetate (85:15). The product eluted after 7.50 minutes as a clear oil (279 mg, 72%).

^{1}H NMR (400 MHz, $CDCl_3$): δ = 0.66 (q, *J* = 8.0 Hz, 6 H), 0.98 (t, *J* = 8.0 Hz, 9 H), 4.80 (s, 2 H), 6.96 (m, 1 H), 7.10 (m, 1 H), 7.18 (m, 1 H), 7.50 (m, 1 H).

^{13}C NMR (100 MHz, $CDCl_3$): δ = 4.6, 6.8, 58.6 (d, $^3J_{C-F}$ = 4.9 Hz), 114.8 (d, $^2J_{C-F}$ = 21.1 Hz), 124.1 (d, $^4J_{C-F}$ = 3.3 Hz), 128.5 (d, $^4J_{C-F}$ = 4.8 Hz), 160.0 (d, $^1J_{C-F}$ = 243.7 Hz).

GC-MS: *m*/*z* (%) = 241 (6) [M + H]$^+$, 219 (4), 212 (27), 184 (100), 163 (6), 153 (76), 139 (6), 105 (53).

Triethyl((4-(trifluoromethyl)benzyl)oxy)silane (8)[25,51]

4-(Trifluoromethyl)benzaldehyde (200 mg, 1.15 mmol) and triethylsilane (200 mg, 1.72 mmol) were stirred in the presence of 1 mol% of the Pd@MTES catalyst (having ca. 3.3% palladium content) (37.0 mg, $1.15\cdot10^{-5}$ mol) under neat conditions and a nitrogen environment for 18 h. The reaction mixture was then purified on a CombiFlash apparatus, on a neutral alumina prepacked column, using a gradient elution from pure hexane to a mixture of hexane/ethyl acetate (85:15). The product eluted after 5.50 minutes as a clear oil (207 mg, 62%).

^{1}H NMR (400 MHz, $CDCl_3$): δ = 0.42 (q, *J* = 8.2 Hz, 2 H), 0.58 (q, *J* = 8.0 Hz, 4 H), 0.79 (t, *J* = 8.0 Hz, 3 H), 0.97 (t, *J* = 8.0 Hz, 6 H), 4.71 (s, 2 H), 7.31 (m, 2 H), 7.50 (m, 2 H).

^{13}C NMR (100 MHz, $CDCl_3$): δ = 4.4, 4.7, 6.4, 6.5, 64.0, 123.9 (d, $^3J_{C-F}$ = 4.7 Hz), 128.5 (d, $^2J_{C-F}$ = 34.8 Hz), 145.5 (d, $^1J_{C-F}$ = 222.5 Hz).

GC-MS: *m*/*z* (%) = 290 (4) [M]$^+$, 274 (15), 261 (27), 203 (46), 184 (21), 169 (100), 118 (38).

Triethyl((4-nitrobenzyl)oxy)silane (9)[45,46]

p-Nitrobenzaldehyde (200 mg, 1.32 mmol) and triethylsilane (231 mg, 2.00 mmol) were stirred in the presence of 1 mol% of the Pd@MTES catalyst (having ca. 3.3% palladium content) (42.7 mg, $1.32\cdot10^{-5}$ mol) in 500 µL of toluene under a nitrogen environment for 18 h. The reaction mixture was then purified on a CombiFlash apparatus, on a neutral alumina prepacked column, using a gradient elution from pure hexane to a mixture of hexane/ethyl acetate (8:2). The product eluted after 7.60 minutes as a clear oil (124 mg, 35%).

^{1}H NMR (400 MHz, $CDCl_3$): δ = 0.70 (q, *J* = 7.8 Hz, 6 H), 1.01 (t, *J* = 7.8 Hz, 9 H), 4.85 (s, 2 H), 7.52 (d, *J* = 8.0 Hz, 2 H), 8.22 (d, *J* = 8.1 Hz, 2 H).

^{13}C NMR (100 MHz, $CDCl_3$): δ = 4.43, 6.72, 63.7, 123.5, 126.4, 127.2, 129.4, 149.0.

GC-MS: *m*/*z* (%) = 268 (2) [M + H]$^+$, 239 (42), 210 (61), 180 (100), 162 (53), 136 (77), 106 (17).

4-(((Triethylsilyl)oxy)methyl)pyridine (10)[47]

Pyridine-4-carbaldehyde (200 mg, 1.87 mmol) and triethylsilane (326 mg, 2.80 mmol) were stirred in the presence of 1 mol% of the Pd@MTES catalyst (having ca. 3.3% palladium content) (60.2 mg, $1.87\cdot10^{-5}$ mol) under neat conditions and a nitrogen environment for 18 h. The reaction mixture was then purified on a CombiFlash apparatus, on a neutral alumina prepacked column, using a gradient elution from pure hexane to a mixture of hexane/ethyl acetate (95:5). The product eluted after 8.20 minutes as a clear oil (163 mg, 39%).

^{1}H NMR (400 MHz, $CDCl_3$): δ = 0.60 (q, *J* = 7.2 Hz, 6 H), 0.91 (t, *J* = 7.2 Hz, 9 H), 4.69 (s, 2 H), 7.20 (d, *J* = 6.3 Hz, 2 H), 8.49 (d, *J* = 6.3 Hz, 2 H).

^{13}C NMR (100 MHz, $CDCl_3$): δ = 3.4, 5.7, 62.2, 119.7, 148.6, 149.5.

GC-MS: *m*/*z* (%) = 224 (20) [M + H]$^+$, 194 (100), 164 (74), 136 (14), 92 (13), 65 (21).

Diethyl((4-methylbenzyl)oxy)silane (13)[52]

p-Tolualdehyde (200 mg, 1.66 mmol) and diethylsilane (220 mg, 2.50 mmol) were stirred in the presence of 1 mol% of the Pd@MTES catalyst (having ca. 3.3% palladium content) (53.7 mg, $1.66\cdot10^{-5}$ mol) under neat conditions and a nitrogen environment for 18 h. The reaction mixture was then purified on a CombiFlash apparatus, on a neutral alumina prepacked column, using a gradient elution from pure hexane to a mixture of hexane/ethyl acetate (95:5). The product eluted after 6.40 minutes as a clear oil (295 mg, 85%).

^{1}H NMR (400 MHz, $CDCl_3$): δ = 0.54 (q, *J* = 7.4 Hz, 4 H), 0.90 (t, *J* = 7.4 Hz, 6 H), 2.25 (s, 3 H), 4.46 (s, 1 H), 4.66 (s, 2 H), 7.04 (d, *J* = 7.4 Hz, 2 H), 7.12 (d, *J* = 7.9 Hz, 2 H).

^{13}C NMR (100 MHz, $CDCl_3$): δ = 4.6, 5.5, 6.0, 20.1, 63.0, 125.4, 127.9, 135.5, 137.0.

GC-MS: *m*/*z* (%) = 208 (37) [M]$^+$, 175 (49), 149 (72), 118 (57), 105 (100), 89 (27).

Diethyl((2-methylbenzyl)oxy)silane (14)[52,53]

o-Tolualdehyde (200 mg, 1.66 mmol) and diethylsilane (220 mg, 2.50 mmol) were stirred in the presence of 1 mol% of the Pd@MTES catalyst (having ca. 3.3% palladium content) (53.7 mg, $1.66\cdot10^{-5}$ mol) under neat conditions and a nitrogen environment for 18 h. The reaction mixture was then purified on a CombiFlash apparatus, on a neutral alumina prepacked column, using a gradient elution from pure hexane to a mixture of hexane/ethyl acetate (95:5). The product eluted after 6.30 minutes as a clear oil (264 mg, 76%).

^{1}H NMR (400 MHz, $CDCl_3$): δ = 0.55 (q, *J* = 7.8 Hz, 4 H), 0.90 (t, *J* = 7.9 Hz, 6 H), 2.21 (s, 3 H), 4.47 (s, 1 H), 4.70 (s, 2 H), 7.09 (m, 3 H), 7.35 (d, *J* = 8.4 Hz, 1 H).

^{13}C NMR (100 MHz, $CDCl_3$): δ = 4.6, 5.5, 6.0, 17.5, 61.4, 124.8, 125.6, 126.0, 128.8, 134.1, 137.8.

GC-MS: *m*/*z* (%) = 208 (23) $[M]^+$, 207 (100) $[M - H]^+$, 177 (17), 149 (20), 105 (25).

Diethyl((4-methoxybenzyl)oxy)silane (15)[52]

p-Anisaldehyde (200 mg, 1.47 mmol) and diethylsilane (194 mg, 2.20 mmol) were stirred in the presence of 1 mol% of the Pd@MTES catalyst (having ca. 3.3% palladium content) (47.4 mg, $1.47\cdot10^{-5}$ mol) under neat conditions and a nitrogen environment for 18 h. The reaction mixture was then purified on a CombiFlash apparatus, on a neutral alumina prepacked column, using a gradient elution from pure hexane to a mixture of hexane/ethyl acetate (95:5). The product eluted after 5.15 minutes as a clear oil (274 mg, 83%).

^{1}H NMR (400 MHz, $CDCl_3$): δ = 0.55 (q, *J* = 7.2 Hz, 4 H), 0.89 (t, *J* = 7.4 Hz, 6 H), 3.72 (s, 3 H), 4.47 (s, 1 H), 4.65 (s, 2 H), 6.79 (d, *J* = 8.6 Hz, 2 H), 7.18 (d, *J* = Hz, 2 H).

^{13}C NMR (100 MHz, $CDCl_3$): δ = 5.4, 5.5, 6.0, 54.3, 63.0, 112.6, 126.8, 132.2, 157.7.

GC-MS: *m*/*z* (%) = 225 (27) $[M + H]^+$, 195 (32), 181 (11), 167 (20), 137 (12), 121 (100).

Diethyl((2-methoxybenzyl)oxy)silane (16)[52,54]

o-Anisaldehyde (200 mg, 1.47 mmol) and diethylsilane (194 mg, 2.20 mmol) were stirred in the presence of 1 mol% of the Pd@MTES catalyst (having ca. 3.3% palladium content) (47.4 mg, $1.47\cdot10^{-5}$ mol) under neat conditions and a nitrogen environment for 18 h. The reaction mixture was then purified on a CombiFlash apparatus, on a neutral alumina prepacked column, using a gradient elution from pure hexane to a mixture of hexane/ethyl acetate (95:5). The product eluted after 6.18 minutes as a clear oil (250 mg, 76%).

^{1}H NMR (400 MHz, $CDCl_3$): δ = 0.55 (q, *J* = 7.3 Hz, 4 H), 0.90 (t, *J* = 7.2 Hz, 6 H), 3.74 (s, 3 H), 4.46 (s, 1 H), 4.75 (s, 2 H), 6.74 (d, *J* = 7.6 Hz, 1 H), 6.90 (t, *J* = 6.8 Hz, 1 H), 7.15 (t, *J* = 7.6 Hz, 1 H), 7.40 (d, *J* = 6.8 Hz, 1 H).

^{13}C NMR (100 MHz, $CDCl_3$): δ = 4.5, 4.6, 6.0, 54.1, 58.2, 108.5, 119.4, 126.0, 126.6, 128.5, 155.1.

GC-MS: *m*/*z* (%) = 224 (45) $[M]^+$, 209 (30), 195 (35), 182 (27), 137 (16), 122 (100).

Diethoxy(methyl)((4-methylbenzyl)oxy)silane (17)[55]

p-Tolualdehyde (200 mg, 1.66 mmol) and methyldiethoxysilane (335 mg, 2.50 mmol) were stirred in the presence of 1 mol% of the Pd@MTES catalyst (having ca. 3.3% palladium content) (53.7 mg, $1.66\cdot10^{-5}$ mol) under neat conditions and a nitrogen environment for 18 h. The reaction mixture was then purified on a CombiFlash apparatus, on a neutral alumina prepacked column, using a gradient elution from pure hexane to a mixture of hexane/ethyl acetate (9:1). The product eluted after 7.08 minutes as a yellowish oil (267 mg, 63%).

^{1}H NMR (400 MHz, $CDCl_3$): δ = 0.14 (s, 3 H), 1.21 (t, *J* = 7.0 Hz, 6 H), 2.32 (s, 3 H), 3.80 (q, *J* = 7.0 Hz, 4 H), 4.79 (s, 2 H), 7.13 (d, *J* = 6.4 Hz, 2 H), 7.23 (d, *J* = 6.4 Hz, 2 H).

^{13}C NMR (100 MHz, $CDCl_3$): δ = 25.2, 28.1, 65.4, 71.4, 133.7, 136.0, 143.8, 144.4.

GC-MS: *m*/*z* (%) = 254 (3) $[M^+]$, 237 (100), 208 (8), 132 (5), 105 (63).

Triisopropyl((4-methylbenzyl)oxy)silane (18)[56]

p-Tolualdehyde (200 mg, 1.66 mmol) and triisopropylsilane (395 mg, 2.50 mmol) were stirred in the presence of 1 mol% of the Pd@MTES catalyst (having ca. 3.3% palladium content) (53.7 mg, $1.66\cdot10^{-5}$ mol) under neat conditions and a nitrogen environment for 18 h. The reaction mixture was then purified on a CombiFlash apparatus, on a neutral alumina prepacked column, using a gradient elution from pure hexane to a mixture of hexane/ethyl acetate (9:1). The product eluted after 6.10 minutes as a clear oil (162 mg, 35%).

^{1}H NMR (400 MHz, $CDCl_3$): δ = 0.97 (d, *J* = 7.3 Hz, 18 H), 1.07 (m, 3 H), 2.25 (s, 3 H), 4.71 (s, 2 H), 7.05 (d, *J* = 7.8 Hz, 2 H), 7.16 (d, *J* = 7.8 Hz, 2 H).

^{13}C NMR (100 MHz, $CDCl_3$): δ = 11.0, 17.0, 20.1, 63.9, 124.8, 127.8, 135.2, 137.6.

GC-MS: *m*/*z* (%) = 278 (3) $[M^+]$, 247 (4), 235 (100), 205 (43), 193 (27), 165 (5), 145 (27), 132 (33), 105 (73).

Triisopropyl((4-methoxybenzyl)oxy)silane (19)[57]

p-Anisaldehyde (200 mg, 1.47 mmol) and triisopropylsilane (349 mg, 2.20 mmol) were stirred in the presence of 1 mol% of the Pd@MTES catalyst (having ca. 3.3% palladium content) (47.4 mg, $1.47\cdot10^{-5}$ mol) under neat conditions and a nitrogen environment for 18 h. The reaction mixture was then purified on a CombiFlash apparatus, on a neutral alumina prepacked column, using a gradient elution from pure hexane to a mixture of hexane/ethyl acetate (9:1). The product eluted after 7.63 minutes as a yellowish oil (182 mg, 42%).

^{1}H NMR (400 MHz, $CDCl_3$): δ = 0.97–1.05 (m, 21 H), 3.61 (s, 3 H), 4.64 (s, 2 H), 6.72 (d, *J* = 8.4 Hz, 2 H), 7.14 (d, *J* = 8.4 Hz, 2 H).

^{13}C NMR (100 MHz, $CDCl_3$): δ = 11.1, 17.0, 54.0, 63.7, 112.5, 126.1, 132.7, 157.6.

GC-MS: *m*/*z* (%) = 294 (10) $[M]^+$, 251 (67), 122 (100).

Triisopropyl((3-methoxybenzyl)oxy)silane (20)[58]

m-Anisaldehyde (200 mg, 1.47 mmol) and triisopropylsilane (349 mg, 2.20 mmol) were stirred in the presence of 1 mol% of the Pd@MTES catalyst (having ca. 3.3% palladium content) (47.4 mg, $1.47\cdot10^{-5}$ mol) under neat conditions and a nitrogen environment for 18 h. The reaction mixture was then purified on a CombiFlash apparatus, on a neutral alumina prepacked column, using a gradient elution from pure hexane to a mixture of hexane/ethyl acetate (9:1). The product eluted after 6.30 minutes as a yellowish oil (186 mg, 43%).

^{1}H NMR (400 MHz, $CDCl_3$): δ = 1.01 (d, *J* = 6.4 Hz, 18 H), 1.05–1.14 (m, 3 H), 3.71 (s, 3 H), 4.74 (s, 2 H), 6.68 (dd, *J* = 2.3, 8.1 Hz, 1 H), 6.81 (d, *J* = 7.6 Hz, 1 H), 6.88 (d, *J* = 2.3 Hz, 1 H), 7.14 (dd, *J* = 7.8, 7.9 Hz, 1 H).

^{13}C NMR (100 MHz, $CDCl_3$): δ = 11.0, 17.0, 54.0, 63.8, 110.1, 111.3, 116.8, 128.1, 142.4, 158.7.

GC-MS: *m*/*z* (%) = 294 (17) $[M]^+$, 251 (78), 223 (54), 193 (2), 121 (100).

Triisopropyl((2-methoxybenzyl)oxy)silane (21)[59]

o-Anisaldehyde (200 mg, 1.47 mmol) and triisopropylsilane (349 mg, 2.20 mmol) were stirred in the presence of 1 mol% of the Pd@MTES catalyst (having ca. 3.3% palladium content) (47.4 mg, $1.47{\cdot}10^{-5}$ mol) under neat conditions and a nitrogen environment for 18 h. The reaction mixture was then purified on a CombiFlash apparatus, on a neutral alumina prepacked column, using a gradient elution from pure hexane to a mixture of hexane/ethyl acetate (9:1). The product eluted after 6.15 minutes as a yellowish oil (138 mg, 32%).

^{1}H NMR (400 MHz, $CDCl_3$): δ = 1.02–1.12 (m, 21 H), 3.72 (s, 3 H), 4.77 (s, 2 H), 6.72 (d, *J* = 7.8 Hz, 1 H), 6.90 (dd, *J* = 6.8, 6.9 Hz, 1 H), 7.12 (dd, *J* = 6.7, 7.5 Hz, 1 H), 7.49 (d, *J* = 6.6 Hz, 1 H).

^{13}C NMR (100 MHz, $CDCl_3$): δ = 11.1, 17.1, 54.0, 59.2, 108.3, 119.4, 125.3, 126.2, 129.1, 154.8.

GC-MS: *m*/*z* (%) = 294 (6) [M]$^+$, 251 (36), 221 (10), 193 (44), 155 (81), 122 (100).

((4-Fluorobenzyl)oxy)triisopropylsilane (23)[60]

p-Fluorobenzaldehyde (200 mg, 1.61 mmol) and triisopropylsilane (383 mg, 2.42 mmol) were stirred in the presence of 1 mol% of the Pd@MTES catalyst (having ca. 3.3% palladium content) (52.0 mg, $1.61{\cdot}10^{-5}$ mol) under neat conditions and a nitrogen environment for 18 h. The reaction mixture was then purified on a CombiFlash apparatus, on a neutral alumina prepacked column, using a gradient elution from pure hexane to a mixture of hexane/ethyl acetate (9:1). The product eluted after 10.2 minutes as a yellowish oil (223 mg, 49%).

^{1}H NMR (400 MHz, $CDCl_3$): δ = 0.99–1.11 (m, 21 H), 4.71 (s, 2 H), 6.92 (dd, $^3J_{H-F}$ = 8.6, *J* = 8.5 Hz, 2 H), 7.22 (dd, $^4J_{H-F}$ = 5.9, *J* = 7.3 Hz, 2 H).

^{13}C NMR (100 MHz, $CDCl_3$): δ = 11.0, 17.0, 63.4, 113.9 (d, $^2J_{C-F}$ = 21.2 Hz), 126.2 (d, $^3J_{C-F}$ = 7.9 Hz), 136.3 (d, $^4J_{C-F}$ = 2.9 Hz), 160.8 (d, $^1J_{C-F}$ = 242.6 Hz).

GC-MS: *m*/*z* (%) = 282 (2) [M]$^+$, 239 (18), 199 (31), 163 (100), 127 (33).

((2-Fluorobenzyl)oxy)triisopropylsilane (24)[60,61]

o-Fluorobenzaldehyde (200 mg, 1.61 mmol) and triisopropylsilane (383 mg, 2.42 mmol) were stirred in the presence of 1 mol% of the Pd@MTES catalyst (having ca. 3.3% palladium content) (52.0 mg, $1.61{\cdot}10^{-5}$ mol) under neat conditions and a nitrogen environment for 18 h. The reaction mixture was then purified on a CombiFlash apparatus, on a neutral alumina prepacked column, using a gradient elution from pure hexane to a mixture of hexane/ethyl acetate (9:1). The product eluted after 10.8 minutes as a yellowish oil (178 mg, 39%).

^{1}H NMR (400 MHz, $CDCl_3$): δ = 0.85 (m, 2 H), 1.02 (d, *J* = 6.7 Hz, 18 H), 1.11 (m, 1 H), 4.82 (s, 2 H), 6.90 (m, 1 H), 7.12 (m, 2 H), 7.51 (m, 1 H).

^{13}C NMR (100 MHz, $CDCl_3$): δ = 11.0, 17.0, 58.0 (d, $^3J_{C-F}$ = 6.4 Hz), 113.5 (d, $^2J_{C-F}$ = 20.7 Hz), 122.9 (d, $^4J_{C-F}$ = 3.2 Hz), 126.9 (d, $^3J_{C-F}$ = 6.8 Hz), 127.1 (d, $^3J_{C-F}$ = 7.9 Hz), 127.7 (d, $^2J_{C-F}$ = 18.5 Hz), 158.5 (d, $^1J_{C-F}$ = 243.3 Hz).

GC-MS: *m*/*z* (%) = 282 (1) [M]$^+$, 242 (13), 239 (23), 207 (8), 189 (29), 163 (100), 127 (31).

Benzyl((4-methoxybenzyl)oxy)dimethylsilane (25)[62]

p-Anisaldehyde (200 mg, 1.47 mmol) and benzyldimethylsilane (331 mg, 2.20 mmol) were stirred in the presence of 1 mol% of the Pd@MTES catalyst (having ca. 3.3% palladium content) (47.4 mg, $1.47{\cdot}10^{-5}$ mol) under neat conditions and a nitrogen environment for 18 h. The reaction mixture was then purified on a CombiFlash apparatus, on a neutral alumina prepacked column, using a gradient elution from pure hexane to a mixture of hexane/ethyl acetate (9:1). The product eluted after 6.30 minutes as a yellowish oil (231 mg, 55%).

^{1}H NMR (400 MHz, $CDCl_3$): δ = 0.18 (s, 6 H), 2.27 (s, 2 H), 3.83 (s, 3 H), 4.67 (s, 2 H), 6.91 (d, *J* = 8.8 Hz, 2 H), 7.12 (m, 3 H), 7.27 (m, 4 H).

^{13}C NMR (100 MHz, $CDCl_3$): δ = –2.2, 26.8, 55.3, 64.8, 113.8, 124.3, 128.1, 128.4, 128.5, 133.0, 139.1, 159.0.

GC-MS: *m*/*z* (%) = 286 (2) [M$^+$], 271 (23), 195 (34), 183 (67), 137 (27), 122 (100).

Benzyl((2-methoxybenzyl)oxy)dimethylsilane (26)[63]

o-Anisaldehyde (200 mg, 1.47 mmol) and benzyldimethylsilane (331 mg, 2.20 mmol) were stirred in the presence of 1 mol% of the Pd@MTES catalyst (having ca. 3.3% palladium content) (47.4 mg, $1.47{\cdot}10^{-5}$ mol) under neat conditions and a nitrogen environment for 18 h. The reaction mixture was then purified on a CombiFlash apparatus, on a neutral alumina prepacked column, using a gradient elution from pure hexane to a mixture of hexane/ethyl acetate (9:1). The product eluted after 6.10 minutes as a yellowish oil (252 mg, 60%).

^{1}H NMR (400 MHz, $CDCl_3$): δ = 0.16 (s, 3 H), 0.21 (s, 3 H), 2.32 (s, 2 H), 3.88 (s, 3 H), 4.82 (s, 2 H), 6.90 (d, *J* = 8.2 Hz, 1 H), 7.04 (m, 1 H), 7.12 (m, 3 H), 7.28 (m, 3 H), 7.47 (d, *J* = 7.2 Hz, 1 H).

^{13}C NMR (100 MHz, $CDCl_3$): δ = –2.4, 1.1, 26.7, 55.2, 60.1, 109.8, 120.5, 124.2, 128.0, 128.1, 128.2, 128.4, 129.2, 139.2, 156.3.

GC-MS: *m*/*z* (%) = 286 [M$^+$] (0.9), 271 (12), 241 (32), 195 (67), 182 (100), 165 (18), 136 (7), 121 (47), 103 (30).

Benzyldimethyl((4-nitrobenzyl)oxy)silane (27)[51,62]

4-Nitrobenzaldehyde (200 mg, 1.32 mmol) and benzyldimethylsilane (298 mg, 1.99 mmol) were stirred in the presence of 1 mol% of the Pd@MTES catalyst (having ca. 3.3% palladium content) (42.7 mg, $1.32{\cdot}10^{-5}$ mol) in 500 µL of toluene under a nitrogen environment for 18 h. The reaction mixture was then purified on a CombiFlash apparatus, on a neutral alumina prepacked column, using a gradient elution from pure hexane to a mixture of hexane/ethyl acetate (8:2). The product eluted after 9.20 minutes as a yellowish oil (168 mg, 42%).

^{1}H NMR (400 MHz, $CDCl_3$): δ = 0.24 (s, 6 H), 2.32 (s, 2 H), 4.79 (s, 2 H), 7.16 (m, 3 H), 7.28 (m, 2 H), 7.45 (d, *J* = 8.4 Hz, 2 H), 8.20 (d, *J* = 8.4 Hz, 2 H).

^{13}C NMR (100 MHz, $CDCl_3$): δ = –2.3, 26.7, 63.8, 123.5, 124.5, 126.6, 128.4, 138.6, 147.1, 148.6.

GC-MS: *m*/*z* (%) = 301 (2) [M$^+$], 287 (6), 211 (55), 183 (23), 153 (72), 137 (100).

Triethyl(1-phenylethoxy)silane (28)[64]

Acetophenone (200 mg, 1.66 mmol) and triethylsilane (290 mg, 2.49 mmol) were stirred in the presence of 1 mol% of the Pd@MTES catalyst (having ca. 3.3% palladium content) (53.6 mg, $1.66{\cdot}10^{-5}$ mol) under neat conditions and a nitrogen environment for 18 h. The reaction mixture was then purified on a CombiFlash apparatus, on a neutral alumina prepacked column, using a gradient elution from pure hexane to a mixture of hexane/ethyl acetate (9:1). The product eluted after 6.30 minutes as a clear oil (126 mg, 32%).

^{1}H NMR (400 MHz, $CDCl_3$): δ = 0.56 (q, *J* = 6.4 Hz, 6 H), 0.91 (t, *J* = 6.4 Hz, 9 H), 1.42 (d, *J* = 7.0 Hz, 3 H), 4.86 (q, *J* = 6.8 Hz, 1 H), 7.19–7.32 (m, 5 H).

^{13}C NMR (100 MHz, $CDCl_3$): δ = 4.9, 6.8, 27.3, 70.7, 125.3, 126.8, 128.1, 147.0.

GC-MS: *m*/*z* (%) = 236 (1) [M$^+$], 222 (12), 207 (100), 164 (2), 135 (23), 103 (100), 77 (39).

Triethyl(1-(2-methoxyphenyl)ethoxy)silane (29)[65]

2′-Methoxyacetophenone (200 mg, 1.33 mmol) and triethylsilane (310 mg, 2.66 mmol) were stirred in the presence of 1 mol% of the Pd@MTES catalyst (having ca. 3.3% palladium content) (42.9 mg, $1.33 \cdot 10^{-5}$ mol) under neat conditions and a nitrogen environment for 18 h. The reaction mixture was then purified on a CombiFlash apparatus, on a neutral alumina prepacked column, using a gradient elution from pure hexane to a mixture of hexane/ethyl acetate (9:1). The product eluted after 7.09 minutes as a yellowish oil (177 mg, 50%).

^{1}H NMR (400 MHz, $CDCl_3$): δ = 0.57 (q, *J* = 6.8 Hz, 6 H), 0.91 (t, *J* = 6.8 Hz, 9 H), 1.37 (d, *J* = 6.4 Hz, 3 H), 3.80 (s, 3 H), 5.23 (q, *J* = 6.4 Hz, 1 H), 6.81 (d, *J* = 6.8 Hz, 1 H), 6.95 (dd, *J* = 6.8, 6.2 Hz, 1 H), 7.18 (dd, *J* = 6.2, 6.0 Hz, 1 H), 7.54 (d, *J* = 6.0 Hz, 1 H).

^{13}C NMR (100 MHz, $CDCl_3$): δ = 4.8, 6.8, 25.7, 55.2, 64.7, 109.8, 120.6, 126.0, 127.4, 135.5, 155.2.

GC-MS: *m*/*z* (%) = 265 (1) [M – H]$^+$, 253 (6), 240 (52), 217 (100), 189 (50), 165 (2), 135 (34), 120 (12), 103 (57).

Funding Information

J.F. acknowledges the financial support from the National Science Foundation (NSF CHE-1954734) and from the Edward G. Schlieder Educational Foundation.

Supporting Information

Supporting information for this article is available online at https://doi.org/10.1055/a-2326-6277.

References

(1) (a) Friend, C. M.; Xu, B. *Acc. Chem. Res.* **2017**, *50*, 517. (b) Wang, Y.; Sun, J.; Tsubaki, N. *Acc. Chem. Res.* **2023**, *56*, 2341. (c) Guo, Z.; Liu, B.; Zhang, Q.; Deng, W.; Wang, Y.; Yang, Y. *Chem. Soc. Rev.* **2014**, *43*, 3480.
(2) (a) Yue, J. *Catal. Today* **2018**, *308*, 3. (b) Vasquez-Cespedes, S.; Betori, R. C.; Cismesia, M. A.; Kirsch, J. K.; Yang, Q. *Org. Process Res. Dev.* **2021**, *25*, 740.
(3) (a) Tuteja, J. *SynOpen* **2023**, *7*, 353. (b) Dutta, S. *Energy Fuels* **2023**, *37*, 2648. (c) Keller, N.; Ivanez, J.; Highfield, J.; Ruppert, A. M. *Appl. Catal., B* **2021**, *296*, 120320.
(4) (a) Baumann, M.; Moody, T. S.; Smyth, M.; Wharry, S. *Org. Process Res. Dev.* **2020**, *24*, 1802. (b) Beckers, O.; Smeets, S.; Lutsen, L.; Maes, W. *J. Mater. Chem. C* **2022**, *10*, 1606. (c) Gutmann, B.; Cantillo, D.; Kappe, C. O. *Angew. Chem. Int. Ed.* **2015**, *54*, 6688.
(5) Duke, B. J.; Akeroyd, E. N.; Bhatt, S. V.; Onyeagusi, C. I.; Bhatt, S. V.; Adolph, B. R.; Fotie, J. *New J. Chem.* **2018**, *42*, 11782.
(6) (a) Cui, Y.; Zhao, Y.; Wu, J.; Hou, H. *Adv. Funct. Mater.* **2023**, *33*, 2302573. (b) Pourmadadi, M.; Ostovar, S.; Eshaghi, M. M.; Rajabzadeh-Khosroshahi, M.; Safakhah, S.; Ghotekar, S.; Rahdar, A.; Diez-Pascual, A. M. *Appl. Organomet. Chem.* **2023**, *37*, e6982. (c) Rezki, M.; Septiani, N. L. W.; Iqbal, M.; Adhika, D. R.; Wenten, I. G.; Yuliarto, B. *J. Electrochem. Soc.* **2022**, *169*, 017504.
(7) Marra, L.; Fusillo, V.; Wiles, C.; Zizzari, A.; Watts, P.; Rinaldi, R.; Arima, V. *Sci. Adv. Mater.* **2013**, *5*, 475.
(8) Ciriminna, R.; Pandarus, V.; Fidalgo, A.; Ilharco, L. M.; Beland, F.; Pagliaro, M. *Org. Process Res. Dev.* **2015**, *19*, 755.
(9) Ciriminna, R.; Pandarus, V.; Gingras, G.; Beland, F.; Pagliaro, M. *ACS Sustainable Chem. Eng.* **2013**, *1*, 249.
(10) John, L.; Janeta, M.; Szafert, S. *New J. Chem.* **2018**, *42*, 39.
(11) (a) Ludwig, J. R.; Schindler, C. S. *Chem* **2017**, *2*, 313. (b) Sruamsiri, D.; Shimojima, A.; Ogawa, M. *ACS Appl. Mater. Interfaces* **2023**, *15*, 41130.
(12) (a) Laird, M.; Herrmann, N.; Ramsahye, N.; Totee, C.; Carcel, C.; Unno, M.; Bartlett, J. R.; Man, M. W. C. *Angew. Chem. Int. Ed.* **2021**, *60*, 3022.
(13) Zhou, H.; Liu, L.; Zhang, W.; Yang, R. *J. Appl. Polym. Sci.* **2023**, *140*, e54378.
(14) (a) Moein, A.; Kebritchi, A. *Silicon* **2023**, *15*, 5845. (b) Hudson, R.; Katz, J. L. *ACS Sustainable Chem. Eng.* **2018**, *6*, 14880.
(15) (a) Bermesheva, E. V.; Alentiev, D. A.; Moskalets, A. P.; Bermeshev, M. V. *Polym. Sci., Ser. B* **2019**, *61*, 314. (b) Zhang, K.; Huang, S.; Zhang, Q.; Zhu, H.; Zhu, S. *Can. J. Chem. Eng.* **2023**, *101*, 4979.
(16) John, L.; Ejfler, J. *Polymers* **2023**, *15*, 1452.
(17) Lamont, C.; Grego, T.; Nanbakhsh, K.; Shah Idil, A.; Giagka, V.; Vanhoestenberghe, A.; Cogan, S.; Donaldson, N. *J. Neural Eng.* **2021**, *18*, 055003.
(18) (a) Bialek, M.; Czaja, K. *Materials* **2023**, *16*, 1876. (b) Liu, C.; Ma, C.; Xie, Q.; Zhang, G. *J. Mater. Chem. A* **2017**, *5*, 15855.
(19) Belancon, M. P.; Sandrini, M.; Zanuto, V. S.; Muniz, R. F. *J. Non-Cryst. Solids* **2023**, *619*, 122548.
(20) (a) Kong, X.; Xi, Z.; Wang, L.; Zhou, Y.; Liu, Y.; Wang, L.; Li, S.; Chen, X.; Wan, Z. *Molecules* **2023**, *28*, 2079. (b) Ojha, G. P.; Kang, G. W.; Kuk, Y.-S.; Hwang, Y. E.; Kwon, O. H.; Pant, B.; Acharya, J.; Park, Y. W.; Park, M. *Nanomaterials* **2023**, *13*, 150. (c) Chakravarty, S.; Teng, M.; Safian, R.; Zhuang, L. *J. Semicond.* **2021**, *42*, 041303.
(21) (a) Bodiford, N. K.; Coffer, J. L. *RSC Smart Mater.* **2017**, *25*, 90. (b) Peng, F.; Cao, Z.; Ji, X.; Chu, B.; Su, Y.; He, Y. *Nanomedicine* **2015**, *10*, 2109. (c) Peng, F.; Su, Y.; Zhong, Y.; Fan, C.; Lee, S.-T.; He, Y. *Acc. Chem. Res.* **2014**, *47*, 612. (d) Peng, H.; Wang, G.; Chang, N.; Wang, Q. *Applications of Porous Silicon Materials in Drug Delivery*, In *Porous Silicon: From Formation to Application: Biomedical and Sensor Applications, Vol. 2, Chap 18*; Korotcenkov, G., Ed.; CRC Press: Boca Raton, **2016**, 337. (e) Zhang, X.-F.; Dong, H.-X.; Chou, Y.-Y. *Appl. Mech. Mater.* **2014**, *618*, 431. (f) Qu, H.; Bhattacharyya, S.; Ducheyne, P. *Adv. Drug Delivery Rev.* **2015**, *94*, 96. (g) Wang, W.; Wang, P.; Tang, X.; Elzatahry, A. A.; Wang, S.; Al-Dahyan, D.; Zhao, M.; Yao, C.; Hung, C.-T.; Zhu, X.; Zhao, T.; Li, X.; Zhang, F.; Zhao, D. *ACS Cent. Sci.* **2017**, *3*, 839.
(22) (a) Sun, J.; Deng, L. *ACS Catal.* **2016**, *6*, 290. (b) Du, X.; Huang, Z. *ACS Catal.* **2017**, *7*, 1227. (c) Obligacion, J. V.; Chirik, P. J. *Nat. Rev. Chem.* **2018**, *2*, 15. (d) Zaranek, M.; Pawluc, P. *ACS Catal.* **2018**, *8*, 9865. (e) Shi, R.; Zhang, Z.; Hu, X. *Acc. Chem. Res.* **2019**, *52*, 1471. (f) Naganawa, Y.; Inomata, K.; Sato, K.; Nakajima, Y. *Tetrahedron Lett.* **2020**, *61*, 151513.
(23) (a) Kumar, A.; Gupta, R.; Mani, G. *Organometallics* **2023**, *42*, 732. (b) Almutairi, N.; Vijjamarri, S.; Du, G. *Catalysts* **2023**, *13*, 665. (c) Thompson, C. V.; Arman, H. D.; Tonzetich, Z. J. *Organometallics* **2022**, *41*, 430. (d) Raya-Baron, A.; Ona-Burgos, P.; Fernandez, I. *ACS Catal.* **2019**, *9*, 5400. (e) Matsubara, K.; Mitsuyama, T.; Shin, S.; Hori, M.; Ishikawa, R.; Koga, Y. *Organometallics* **2021**, *40*, 1379.
(24) Chouthaiwale, P. V.; Rawat, V.; Sudalai, A. *Tetrahedron Lett.* **2012**, *53*, 148.

(25) (a) Eckstorff, F.; Zhu, Y.; Maurer, R.; Mueller, T. E.; Scholz, S.; Lercher, J. A. *Polymer* **2011**, *52*, 2492. (b) Feher, F. J.; Terroba, R.; Jin, R.-Z.; Wyndham, K. D.; Lucke, S.; Brutchey, R.; Nguyen, F. *Polym. Mater. Sci. Eng.* **2000**, *82*, 301. (c) Feher, F. J.; Soulivong, D.; Eklund, A. G.; Wyndham, K. D. *Chem. Commun.* **1997**, 1185.
(26) Bassindale, A. R.; Liu, Z.; MacKinnon, I. A.; Taylor, P. G.; Yang, Y.; Light, M. E.; Horton, P. N.; Hursthouse, M. B. *Dalton Trans.* **2003**, 2945.
(27) Grzelak, M.; Marciniec, B. *Chem. Asian J.* **2020**, *15*, 2437.
(28) (a) Bharathi, S.; Fishelson, N.; Lev, O. *Langmuir* **1999**, *15*, 1929. (b) Fidalgo, A.; Ciriminna, R.; Ilharco, L. M.; Pagliaro, M. *Chem. Mater.* **2005**, *17*, 6686.
(29) (a) Janeta, M.; John, L.; Ejfler, J.; Szafert, S. *Chem. Eur. J.* **2014**, *20*, 15966. (b) Janeta, M.; John, L.; Ejfler, J.; Szafert, S. *RSC Adv.* **2015**, *5*, 72340.
(30) (a) D'Souza, L.; Sampath, S. *Langmuir* **2000**, *16*, 8510. (b) Devarajan, S.; Bera, P.; Sampath, S. *J. Colloid Interface Sci.* **2005**, *290*, 117.
(31) Hanprasit, S.; Tungkijanansin, N.; Prompawilai, A.; Eangpayung, S.; Ervithayasuporn, V. *Dalton Trans.* **2016**, *45*, 16117.
(32) (a) O'Hare, L.-A.; Parbhoo, B.; Leadley, S. R. *Surf. Interface Anal.* **2004**, *36*, 1427. (b) Kato, H.; Takemura, S.; Takakuwa, N.; Ninomiya, K.; Watanabe, T.; Watanabe, Y.; Nanba, N.; Hiramatsu, T. *J. Vac. Sci. Technol., A* **2006**, *24*, 1505.
(33) (a) Bashouti, M. Y.; Paska, Y.; Puniredd, S. R.; Stelzner, T.; Christiansen, S.; Haick, H. *Phys. Chem. Chem. Phys.* **2009**, *11*, 3845. (b) Puniredd, S. R.; Assad, O.; Haick, H. *J. Am. Chem. Soc.* **2008**, *130*, 9184. (c) Puniredd, S. R.; Assad, O.; Haick, H. *J. Am. Chem. Soc.* **2008**, *130*, 13727.
(34) (a) Zhang, F.-B.; Li, H.-L. *Carbon* **2006**, *44*, 3195. (b) Zhang, Q.-L.; Feng, J.-X.; Wang, A.-J.; Wei, J.; Feng, J.-J. *RSC Adv.* **2014**, *4*, 52640. (c) Ju, P.; Chen, J.; Chen, A.; Chen, L.; Yu, Y. *ACS Sustainable Chem. Eng.* **2017**, *5*, 2516.
(35) (a) Kunai, A.; Sakurai, T.; Toyoda, E.; Ishikawa, M.; Yamamoto, Y. *Organometallics* **1994**, *13*, 3233. (b) Ferreri, C.; Costantino, C.; Chatgilialoglu, C.; Boukherroub, R.; Manuel, G. *J. Organomet. Chem.* **1998**, *554*, 135.
(36) Rasmussen, A. M. H.; Hammer, B. *J. Chem. Phys.* **2012**, *136*, 174701.
(37) Reuter, K.; Scheffler, M. *Phys. Rev. B.* **2001**, *65*, 03540.
(38) Khezeli, F.; Plaisance, C. *J. Phys. Chem. A.* **2024**, *128*, 1576.
(39) Kresse, G.; Furthmueller, J. *Phys. Rev. B: Condens. Matter Mater. Phys.* **1996**, *54*, 11169.
(40) Wellendorff, J.; Lundgaard, K. T.; Moegelhoej, A.; Petzold, V.; Landis, D. D.; Noerskov, J. K.; Bligaard, T.; Jacobsen, K. W. *Phys. Rev. B: Condens. Matter Mater. Phys.* **2012**, *85*, 235141.
(41) (a) Henkelman, G.; Uberuaga, B. P.; Jonsson, H. *J. Chem. Phys.* **2000**, *113*, 9901. (b) Henkelman, G.; Jonsson, H. *J. Chem. Phys.* **2000**, *113*, 9978.
(42) Henkelman, G.; Jonsson, H. *J. Chem. Phys.* **1999**, *111*, 7010.
(43) Dong, H.; Berke, H. *Adv. Synth. Catal.* **2009**, *351*, 1783.
(44) (a) Chauvier, C.; Thuery, P.; Cantat, T. *Angew. Chem. Int. Ed.* **2016**, *55*, 14096. (b) Diez-Gonzalez, S.; Scott, N. M.; Nolan, S. P. *Organometallics* **2006**, *25*, 2355.
(45) Chatterjee, B.; Gunanathan, C. *Chem. Commun.* **2014**, *50*, 888.
(46) Rawat, S.; Bhandari, M.; Porwal, V. K.; Singh, S. *Inorg. Chem.* **2020**, *59*, 7195.
(47) Do, Y.; Han, J.; Rhee, Y. H.; Park, J. *Adv. Synth. Catal.* **2011**, *353*, 3363.
(48) Teci, M.; Lentz, N.; Brenner, E.; Matt, D.; Toupet, L. *Dalton Trans.* **2015**, *44*, 13991.
(49) Andrews, R. J.; Chitnis, S. S.; Stephan, D. W. *Chem. Commun.* **2019**, *55*, 5599.
(50) Rubio, M.; Campos, J.; Carmona, E. *Org. Lett.* **2011**, *13*, 5236.
(51) Liberman-Martin, A. L.; Bergman, R. G.; Tilley, T. D. *J. Am. Chem. Soc.* **2015**, *137*, 5328.
(52) Hua, Y.; Jung, S.; Roh, J.; Jeon, J. *J. Org. Chem.* **2015**, *80*, 4661.
(53) Simmons, E. M.; Hartwig, J. F. *J. Am. Chem. Soc.* **2010**, *132*, 17092.
(54) (a) Tondreau, A. M.; Lobkovsky, E.; Chirik, P. J. *Org. Lett.* **2008**, *10*, 2789. (b) Royo, B.; Sortais, J.-B.; Darcel, C.; Uhl, W.; Berke, H.; Fukuzawa, S.-I. *Eur. J. Inorg. Chem.* **2012**, 1002.
(55) (a) Maas, L. M.; Fasting, C.; Vossnacker, P.; Limberg, N.; Golz, P.; Mueller, C.; Riedel, S.; Hopkinson, M. N. *Angew. Chem. Int. Ed.* **2024**, *63*, e202317770. (b) Miyazaki, K.; Nakata, K. *J. Org. Chem.* **2022**, *87*, 10509.
(56) Henry, A. T.; Nanan, D. A. R.; Baines, K. M. *Dalton Trans.* **2023**, *52*, 10363.
(57) (a) Davies, H. M. L.; Hedley, S. J.; Bohall, B. R. *J. Org. Chem.* **2005**, *70*, 10737. (b) Khalafi-Nezhad, A.; Fareghi Alamdari, R.; Zekri, N. *Tetrahedron* **2000**, *56*, 7503.
(58) (a) Liu, G.; Li, P. *Synlett* **2023**, *34*, 2447. (b) Lipshutz, B. H.; Keith, J. S. *Tetrahedron Lett.* **1998**, *39*, 2495. (c) Qi, Z.-C.; Li, Y.; Wang, J.; Ma, L.; Wang, G.-W.; Yang, S.-D. *ACS Catal.* **2023**, *13*, 13301.
(59) (a) Cruz, T. F. C.; Veiros, L. F.; Gomes, P. T. *Inorg. Chem.* **2022**, *61*, 1195. (b) Evans, P. A.; Longmire, J. M.; Modi, D. P. *Tetrahedron Lett.* **1995**, *36*, 3985.
(60) Marzi, E.; Spitaleri, A.; Mongin, F.; Schlosser, M. *Eur. J. Org. Chem.* **2002**, 2508.
(61) Panigrahi, A.; Whitaker, D.; Vitorica-Yrezabal, I. J.; Larrosa, I. *ACS Catal.* **2020**, *10*, 2100.
(62) Arii, H.; Nakao, K.; Masuda, H.; Kawashima, T. *ACS Omega* **2022**, *7*, 5166.
(63) Dorsey, C. L.; Gabbai, F. P. *Organometallics* **2008**, *27*, 3065.
(64) (a) Edlova, T.; Normand, A. T.; Cattey, H.; Brandes, S.; Wu, Y.; Antonangelo, A.; Theron, B.; Bonnin, Q.; Carta, M.; Le Gendre, P. *Organometallics* **2023**, *42*, 1166. (b) Jiang, H.-J.; Simon, H. D. A.; Irran, E.; Klare, H. F. T.; Oestreich, M. *Organometallics* **2023**, *42*, 48.
(65) (a) Eaborn, C.; Odell, K.; Pidcock, A. *J. Organomet. Chem.* **1973**, *63*, 93. (b) Yigit, B.; Yigit, M.; Ozdemir, I. *Inorg. Chim. Acta* **2017**, *467*, 75. (c) Yigit, M.; Oezdemir, I.; Cetinkaya, B.; Cetinkaya, E. *J. Mol. Catal. A: Chem.* **2005**, *241*, 88.

